Pergamon

Geochimica et Cosmochimica Acta, Vol. 65, No. 9, pp. 1499–1527, 2001

0016-7037/01 $20.00 + .00

PII S0016-7037(00)00626-8

Geochemistry of xenolithic eclogites from West Africa, Part I: A link between low MgO eclogites and Archean crust formation

MATTHIAS G. BARTH,[1*,†] ROBERTA L. RUDNICK,[1,‡] INGO HORN,[1,§] WILLIAM F. MCDONOUGH,[1,‡] MICHAEL J. SPICUZZA,[2] JOHN W. VALLEY,[2] and STEPHEN E. HAGGERTY[3]

[1]Department of Earth and Planetary Sciences, Harvard University, 20 Oxford Street, Cambridge, MA 02138, USA
[2]Department of Geology and Geophysics, University of Wisconsin, 1215 W. Dayton Street, Madison, WI 53706, USA
[3]Department of Geosciences, University of Massachusetts, Morrill Science Center, Amherst, MA 01003, USA

(*Received May* 17, 2000; *accepted in revised form November* 15, 2000)

Abstract—Oxygen isotope, mineral trace element, and measured and reconstructed whole rock compositions are reported for low MgO (6–13 wt.% MgO in the whole rock) eclogite xenoliths from the Koidu kimberlite complex, Sierra Leone. The $\delta^{18}O$ values of garnet (4.7–6.8‰), determined by laser fluorination on clean mineral separates, extend beyond the range for mantle peridotites. All low MgO eclogites have reconstructed trace element patterns that are depleted in Ba, Th, U, and light rare earth element (LREE), with jadeite-rich samples having more variable trace element patterns than jadeite-poor samples. These observations, coupled with low SiO_2 contents, and Nb-rich but LREE-depleted reconstructed whole rock compositions, suggest the low MgO eclogites are remnants of altered oceanic crust that was partially melted during subduction. Partial melting of a mafic protolith at high pressure (leaving a garnet-bearing residue) is the preferred model to explain the origin of Archean tonalite-trondhjemite-granodiorite (TTG) suites, which make up large portions of the crust in Archean cratons. We therefore suggest that the Koidu low MgO eclogites may be residues from Archean continental crust formation. *Copyright © 2001 Elsevier Science Ltd*

1. INTRODUCTION

Eclogite xenoliths are minor but ubiquitous constituents of mantle xenolith suites brought up by kimberlites in Archean (and Proterozoic) cratons. High equilibration temperatures and the presence of diamond in some eclogite xenoliths suggest derivation from the upper mantle. However, the origin of their protoliths and the subsequent metamorphic evolution of these bi-mineralic rocks are less certain. The different hypotheses proposed for the origin of eclogite xenoliths can be divided into two groups. According to the "mantle" hypothesis, eclogites are produced by high-pressure crystallization from peridotite-generated magmas that ascend through the lithosphere (Smyth et al., 1989; Caporuscio and Smyth, 1990). The "crustal" hypothesis argues that eclogites are remnants of subducted (Archean?) oceanic crust, which may or may not have been through a melting episode associated with subduction (Helmstaedt and Doig, 1975; MacGregor and Manton, 1986; Taylor and Neal, 1989; Ireland et al., 1994; Jacob et al., 1994). A variant of the crustal hypothesis, which has not been widely explored, is that eclogites may be products of metamorphism of mafic lower continental crust, i.e., products of isobaric cooling at high pressure of gabbroic to anorthositic protoliths (Pearson et al., 1991; El Fadili and Demaiffe, 1999).

Evidence cited in support of the mantle hypothesis includes mineralogic layering, cumulate textures, exsolution of garnet from pyroxene, mantle-like oxygen isotope signatures (Smyth et al., 1989; Snyder et al., 1997), and high Cr_2O_3 contents in some xenolithic eclogites (Taylor and Neal, 1989).

The most compelling evidence for the crustal origin of eclogite xenoliths are oxygen isotope compositions that deviate from established peridotitic values, i.e., whole rock $\delta^{18}O$ values that lie beyond 5.5 ± 0.4‰ (Mattey et al., 1994a), but within the range of oxygen isotopes observed in the basaltic sections of ophiolites (see Muehlenbachs, 1986). The fractionation of oxygen isotopes requires low-temperature processes at or close to the surface of the Earth (Clayton et al., 1975). Therefore, samples from the upper mantle with $\delta^{18}O$ outside the mantle range are interpreted either as parts of subducted slabs or as having been contaminated with melts or fluids from subducted slabs. Similar arguments can be made based on carbon isotopes (see Schulze et al., 1997). Moreover, high Al contents of some xenolithic eclogites (manifested by the occurrence of accessory phases such as kyanite and corundum) have been cited as evidence for low-pressure crystallization of plagioclase-rich protoliths (crustal pressures rather than upper mantle) (Jacob et al., 1998; Jacob and Foley, 1999).

In addition to stable isotopes, trace element geochemistry is a powerful tool with which to investigate the concealed evolutionary record of eclogites and to constrain possible precursors. However, a significant problem in any geochemical study of eclogite xenoliths is to determine the pristine, preentrainment composition of these rocks. All eclogite xenoliths exhibit variable degrees of alteration produced by partial melting, metasomatism and/or by interaction with their kimberlitic hosts (Ireland et al., 1994; McCormick et al., 1994; Harte and Kirkley, 1997; Snyder et al., 1997). In general, omphacite is affected more severely than garnet (Taylor and Neal, 1989; Fung and Haggerty, 1995), with kyanite-bearing eclogites showing the

*Author to whom correspondence should be addressed (barth@eps.harvard.edu).
† *Present address:* Utrecht University, Faculty of Earth Sciences, Dept. of Petrology, Budapestlaan 4 3584 CD Utrecht, The Netherlands (barth@geo.uu.nl).
‡ *Present address:* Department of Geology, University of Maryland, College Park, MD 20742, USA.
§ *Present address:* Laboratory for Inorganic Chemistry, ETH Zürich, Universitätsstraße 6, CH-8092 Zürich, Switzerland.

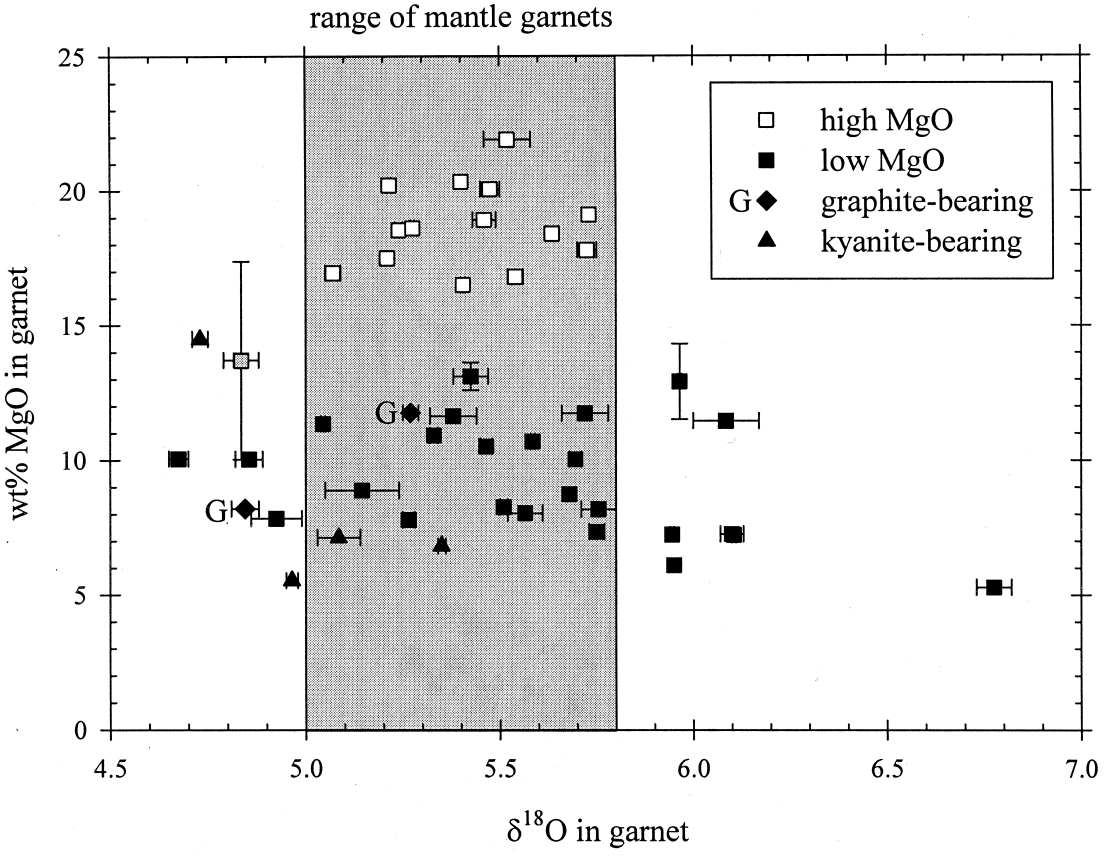

Fig. 1. MgO in garnet vs. $\delta^{18}O$ in garnet for Koidu eclogites. Open squares represent high MgO eclogites; solid symbols show low MgO eclogites. The gray square denotes the transitional eclogite KEC 86-19. Solid squares are bi-mineralic eclogites, solid diamonds are graphite-bearing eclogites (G), and solid triangles are kyanite-bearing eclogites. Horizontal error bars show average reproducibility (½ of the difference between 2 separate measurements); vertical error bars indicate mineral zoning. The gray field depicts the range of mantle garnets that is shifted towards lighter isotopic composition by 0.1‰ relative to the whole rock mantle range due to the fractionation between garnet and whole rock.

highest degrees of alteration (Harte and Kirkley, 1997; Snyder et al., 1997). To see through these effects of alteration, the original whole rock composition must be calculated from the unaltered parts of primary mantle phases. Recent work has utilized in situ trace element measurements for this purpose (e.g., Jerde et al., 1993; Ireland et al., 1994; Harte and Kirkley, 1997; Jacob and Foley, 1999).

Xenolithic eclogites from the Koidu kimberlite complex in Sierra Leone, West Africa, fall into two groups, based on their major element and mineral chemistry (Fig. 1) (Hills and Haggerty, 1989; Fung and Haggerty, 1995): a high MgO group (>16 wt.% MgO) and a low MgO group (6–13 wt.% MgO). It has recently been suggested that the Koidu low MgO eclogites have complementary major element compositions to granitoids from the West African Craton, indicating that both were derived from a common basaltic parent rock with a composition similar to greenstone belt basalts in Sierra Leone (Rollinson, 1997). To investigate this possibility and to constrain the origin(s) and evolution of the Koidu eclogites, we have undertaken an oxygen isotope and trace element study of these rocks. This paper reports the oxygen isotopic compositions and the trace element compositions of low MgO eclogites previously studied by Hills and Haggerty (1989) and Fung and Haggerty (1995). Chemical and isotopic characterization and the genesis of the high MgO eclogites will be presented in a second paper.

2. GEOLOGICAL BACKGROUND AND SAMPLE DESCRIPTION

The Mesozoic Koidu kimberlite complex is located on the Man Shield in West Africa, which lies near the former center of a Precambrian craton that was rifted apart by the opening of the Atlantic Ocean in the Mesozoic to form the West African Craton and the Guyana Shield in South America. The Man Shield is situated in the southern West African Craton and has been divided into three age provinces (Macfarlane et al., 1981): Leonean (~3.0 Ga), Liberian (~2.7 Ga), and Eburnian (~2.0 Ga). However, due to the limited radiometric dating (Rb-Sr and Pb-Pb whole rock) there is a debate as to whether the Leonean and the Liberian are two separate events or a single, long-lived event (Williams, 1978). A younger Pan-African age province defines a tectonic event at ~550 Ma in the coastal belt of Sierra Leone and Liberia.

The Archean basement (Leonean and Liberian provinces) of Sierra Leone is typical of granite-greenstone terrains found in ancient continental nuclei. The older tonalite-trondhjemite-

Table 1. USGS reference glass standards BCR-2g and BIR-1g analyzed by LA-ICP-MS during the course of this study.

	Isotope analyzed	NIST 610 reference value	NIST 612 reference value	BCR-2g reference value	BCR-2g ppm	RSD %	*n*	BIR-1g reference value	BIR-1g ppm	RSD %	*n*
Sc	45	441.1	41.05	32.6	35.1	7.9	68	44.0	46.1	8.9	28
TiO_2 (wt.%)	49	0.07	0.01	2.24	2.54	10.3	68	1.06	1.10	13.4	28
V	51	441.7	37.56	407	423	6.9	62	339	332	4.8	28
Cr	52	405.2	34.9	16	17	19.7	54	382	403	5.7	26
MnO (wt.%)	55	0.06	0.01	0.18	0.20	9.1	44	0.16	0.19	7.3	28
Ni	60	443.9	38.8	13	13	18.8	24	175	188	12.7	28
Zn	66	456.3	37.92	130	163	12.2	14	71	98	9.4	16
Ga	69	438.1	35.88	22	22	6.8	10	16	16	4.2	4
Rb	85	431.1	31.06	47.5	48.6	10.2	64	0.20	0.22	28.3	4
Sr	88	497.4	75.33	337	318	5.2	66	104	102	5.0	28
Y	89	449.9	36.57	32.5	31.5	7.9	66	13.3	13	7.2	28
Zr	90	439.9	35.18	176	165	7.9	66	11.9	12	6.9	28
Nb	93	419.4	38.9	13.1	11.7	8.1	66	0.47	0.49	18.8	20
Mo	95	376.8	38.30	287	263	12.0	14	0.5	b. d.		
Sn	118	396.3	37.67	2.7	4.3	20.5	10	0.54	2.87	23.4	3
Sb	121	368.5	38.44	0.62	b. d			0.58	0.63	24.5	6
Cs	133	360.9	41.8	1.19	1.16	13.8	51	0.008	b. d.		
Ba	138	424.1	38.94	684	647	7.5	52	6.2	6.5	6.8	12
La	139	457.4	35.68	25.3	23.9	5.1	52	0.59	0.61	8.7	12
Ce	140	447.8	37.91	53.6	49.3	7.7	66	1.87	1.80	9.5	28
Pr	141	429.8	37.45	6.83	6.40	6.5	18		n. d.		
Nd	146	430.8	34.6	28.6	26.8	5.6	52	2.3	2.2	6.2	10
Sm	147	450.5	36.8	6.67	6.29	8.4	65	1.01	1.05	12.2	23
Eu	151	461.1	34.4	2.00	1.80	8.1	52	0.48	0.52	12.9	12
Gd	157	419.9	36.95	6.80	6.15	9.2	46	1.64	1.80	9.3	12
Tb	159	442.8	36.93	1.04	0.95	7.5	18		n. d.		
Dy	162	426.5	35.97	6.38	6.13	8.7	65	2.33	2.29	10.3	26
Ho	165	449.4	37.27	1.29	1.19	8.3	24		n. d.		
Er	166	426	37.91	3.66	3.48	9.9	52	1.48	1.65	10.7	12
Tm	169	420.1	37.33	0.54	0.49	10.3	18		n. d.		
Yb	174	461.5	38.14	3.34	3.17	10.3	65	1.48	1.51	9.9	24
Lu	175	434.7	37.2	0.51	0.48	12.8	52	0.23	0.23	14.1	14
Hf	178	417.7	38.14	4.8	4.8	11.1	64	0.46	0.55	13.9	21
Ta	181	376.6	39.33	0.78	0.72	13.7	66	0.031	0.031	24.1	8
W	182	445.3	39.55	0.44	0.70	30.4	12	0.2	b. d.		
Pb	208	413.3	38.96	10.3	11.0	9.4	41	2.85	3.54	12.4	16
Th	232	450.6	36.66	5.98	5.55	9.8	65	0.025	0.033	26.6	15
U	238	457.1	36.66	1.7	1.6	11.5	65	0.022	0.029	26.1	12

Notes to Table 1:

Reference values from Simon E. Jackson's Lamtrace© with updates from Pearce et al. (1997) for NIST 610 and NIST 612, and from Reid et al. (1999) for Zr and Hf in BCR-2g.

All concentrations are given in ppm (μg/g) except TiO_2 and MnO in wt.%. n. d. = not determined; b. d. = below detection limit.

granodiorite (TTG) gneisses (~2.9 Ga) (Beckinsale et al., 1980; Barth et al., 1999) form between 60 and 70% of the outcrop area and are the major rock type of the Man Shield. Younger granites (2.7–2.8 Ga) intrude the margins of the greenstone belts or occur as thick sheets cross-cutting the greenstone belts at high structural levels. The composition of the TTG gneisses range from diorite to granodiorite (Rollinson, 1978). The Koidu kimberlite complex occurs in the interior of this basement. Country rocks to the kimberlites include amphibolite-facies migmatites, TTG gneisses, ironstones, and ultramafic suites.

Hills and Haggerty (1989) and Fung and Haggerty (1995) describe the petrography and report mineral chemical data for 87 eclogite xenoliths and whole rock XRF major and trace element data for 25 of these samples from the Koidu pipes. The high MgO group (>16 wt.% MgO) is essentially bi-mineralic, with only minor ilmenite, and/or sulfide occurring in addition to garnet and omphacite. The low MgO group (6–13 wt.% MgO) commonly contains accessory phases such as kyanite, graphite, quartz (after coesite), diamond, amphibole, and/or corundum plus rutile, ilmenite, and/or sulfides in addition to garnet and omphacite. Generally, both high and low MgO eclogites fall into group II eclogites of McCandless and Gurney (1989), i.e., low Na garnets and low K omphacite, except for the diamond-bearing eclogites and a single graphite-bearing eclogite that fall into group I.

The Koidu eclogites range from nearly pristine rocks with alteration restricted to grain boundaries (e.g., KEC 81-5) to samples with highly altered, opaque clinopyroxene with small relict areas of pristine omphacite in the centers of crystals (e.g., KEC 91-1) (see Fig. 1 of Hills and Haggerty, 1989). Numerous secondary minerals occur in veins within the more altered eclogites. These minerals include phlogopite, amphibole, plagioclase, ilmenite, rutile, sulfide, spinel, and carbonates. Thus, rutile occurs both as primary and secondary phase. Secondary (metasomatic) rutile is distinguished by much higher and het-

Table 2. Oxygen isotopic composition of Koidu eclogite mineral separates determined by laser fluorination (all samples have KEC prefix).

Sample	$\delta^{18}O_{SMOW}$	1σ	Jadeite in cpx [mol.%]	Sample	$\delta^{18}O_{SMOW}$	1σ	Jadeite in cpx [mol.%]
Low MgO garnets—bi-mineralic eclogites				*Low MgO garnets—graphite-bearing eclogites*			
80-A2	5.75	0.02	27%	86-12	4.85	0.04	39%
81-3	5.27	0.01	36%	86-70	5.27	0.02	27%
81-4	5.05	0.01	23%				
81-5	5.57	0.04	6%	*Low MgO garnet—kyanite-bearing eclogites*			
81-7	5.59	0.00	33%				
81-8	5.15	0.10	43%	86-1	4.73	0.02	27%
81-10A	5.72	0.06	45%	86-3	4.97	0.02	49%
81-18	5.95	—	29%	86-4	5.09	0.05	48%
81-21	6.09	0.08	34%	85-74B	5.35	0.01	45%
86-6	5.95	0.01	27%				
86-13	5.51	0.01	32%	*kyanite*			
86-14	5.68	0.00	25%				
86-34	5.38	0.06	45%	86-3	5.56	0.02	
86-36	5.97	0.01	38%	86-4	5.48	0.02	
86-56	5.33	0.01	24%	86-74B	5.70	0.11	
86-71A	4.86	0.03					
91-2	5.70	0.02	31%	*Clinopyroxene*			
91-4	4.68	0.02	27%				
91-7	5.43	0.04		86-90	5.12	0.04	
Core			47%	81-5	5.44	0.01	
Rim			74%	91-2	5.73	0.08	
91-11	4.93	0.06	32%				
91-13	5.47	0.02	30%	*Garnet standard UWG-2*			
91-20	5.76	0.05	22%				
91-22	6.11	0.00	26%	*1/22/98*	5.90	0.06	($n = 3$)
91-23	6.10	0.03	27%	*6/2/99*	5.79	0.10	($n = 3$)
91-58	6.78	0.05	37%	*6/3/99*	5.79	0.05	($n = 3$)

All values are avergaes of two measurements except for KEC 81-18, which is a single measurement. 1σ is the average reproducibility, i.e., 1/2 of the difference between two separate measurements. Samples are corrected to garnet standard UWG-2 = 5.8‰ (Valley et al., 1995).

erogeneous Nb and Ta contents and occasionally by a skeletal texture. Of the samples analyzed by laser ablation inductively coupled plasma-mass spectrometry (LA-ICP-MS), only samples KEC 81-10A, KEC 81-18, and KEC 81-21 contain metasomatic rutile. Based on textures, trace element homogeneity, and evidence for equilibrium between rutile and primary silicates, all rutiles reported in Table 5 and in Rudnick et al. (2000) are considered primary.

The Koidu eclogites show a large range of textures, estimated equilibration temperatures, and pressures, extending from 760°C at 2.8 GPa to 1188°C at 5 GPa, using the Ellis and Green (1979) geothermometer and the Kalahari geotherm of Rudnick and Nyblade (1999). The P-T ranges of the high and low MgO eclogites differ significantly (Hills and Haggerty, 1989; Fung and Haggerty, 1995); many high MgO eclogites record conditions between 1080 and 1130°C and 4.0 and 4.5 GPa, whereas the low MgO eclogites cluster between 880 and 930°C and 3.3 and 3.6 GPa.

3. ANALYTICAL METHODS

Mineral separates for laser fluorination oxygen isotope ratio analysis were prepared by standard procedures, including initial crushing in alumina ceramics followed by magnetic separation. Purity of samples was ensured by hand picking, with sample weights for each analysis ranging between 1 and 3 mg. Oxygen isotope ratios were measured at the University of Wisconsin, Madison, using a laser-assisted fluorination technique described by Valley et al. (1995). This method provides high oxygen yields for refractory minerals like garnet. In most cases repeat analyses fall within 0.1‰ of each other, demonstrating the good reproducibility of the technique and the purity of the mineral separates. Measured values were corrected (≤0.1‰) based on three to four analyses of garnet standard UWG-2 at the start of each day (Table 2) (Valley et al., 1995). Corrected values are reported relative to V-SMOW (Coplen, 1996).

Whole rock trace element compositions were determined by ICP-MS. Samples were dissolved in a mixture of ultrapure, concentrated $HF–HNO_3$ and then spiked with a mixed multi-element/enriched isotope internal standard solution before analysis, following the technique of Eggins et al. (1997). Complete dissolution of the samples was ensured by the use of conventional oven bombs. Analyses were performed on a Fisons (VG Elemental) PQ II + in pulse counting mode (three points per peak). Sensitivity of the instrument was on average ~50 MHz (million counts per second per ppm) for ^{115}In. Standard data and typical precision are reported in Barth et al. (2000).

Trace element compositions of garnets, omphacites, rutiles, and ilmenites were determined by LA-ICP-MS, utilizing both a home-built excimer system (Horn et al., 2000), and later, the Merchantek DUV system, which was developed from our prototype design. Ablation is achieved by a 193 nm Ar-F excimer laser system using a pulse repetition rate of 10 Hz and pulse energy of ≤0.5 mJ (Horn et al., 2000). Analyses were performed in pulse counting mode (one point per peak); dwell time and quadrupole settling time were set to 10 and 5 ms, respectively. Data reduction follows the procedure outlined in Longerich et al. (1996). The amount of material ablated in laser sampling is different for each spot analysis. Consequently, the detection limits are different for each spot and are calculated for each individual acquisition. Typical pit diameters and ablation time for silicates were ~150 μm and 60 s, respectively, resulting in detection limits of 20 ppb for Ta, Th, and U, 50 ppb for the REE (rare earth elements), 0.5 ppm for Rb and Sr, and 1 ppm for Sc. ^{44}Ca and ^{49}Ti were used as internal standards for silicate and oxide analyses, respectively. For our analyses we

Table 3. Trace element composition of garnets determined by LA-ICP-MS.

Sample	**KEC 80-A2** Low jadeite		**KEC 81-4** Low jadeite		**KEC 81-5** Low jadeite		**KEC 81-18** Low jadeite		**KEC 86-6** Low jadeite		**KEC 86-56** Low jadeite	
Spots	$n = 10$	1σ	$n = 7$	1σ	$n = 7$	1σ	$n = 7$	1σ	$n = 7$	1σ	$n = 7$	1σ
Sc	66.5	2.5	50.2	1.9	63.5	2.2	66.9	2.6	73.8	2.2	73.1	2.8
V	203	5	n.d.		179	9	207	31	195	15	161	12
Cr	361	9	n.d.		715	52	414	42	369	9	347	10
Ni	19.8	1.7	n.d.		10.6	1.4	4.7	0.2	<30		83.1	6.0
Ga	n.d.		n.d.		n.d.		n.d.		13.3	0.8	13.0	0.6
Rb	<0.3		<0.3		<0.2		<0.3		<0.5		<1	
Sr	0.45	0.22	<0.2		0.16	0.03	0.39	0.03	0.21	0.01	0.30	0.02
Y	32.8	1.6	35.1	2.4	32.7	1.0	36.4	1.0	31.8	0.3	30.0	1.2
Zr	5.66	0.42	3.01	0.61	4.65	0.24	12.8	0.1	13.8	0.5	12.4	0.4
Nb	<0.2		<0.2		<0.1		<0.03		<0.5		<0.6	
La	<0.05		0.006	—	<0.03		0.012	0.001	<0.05		<0.06	
Ce	0.13	0.01	0.065	0.024	0.074	0.011	0.20	0.04	0.088	0.012	0.10	0.01
Pr	0.11	0.01	n.d.		0.056	0.006	0.14	0.01	n.d.		n.d.	
Nd	1.48	0.12	0.29	0.07	1.01	0.03	2.07	0.13	1.46	0.06	1.15	0.06
Sm	2.00	0.16	0.56	0.02	1.49	0.07	2.38	0.16	1.97	0.10	1.76	0.16
Eu	0.88	0.08	0.40	0.05	0.80	0.02	1.06	0.05	0.86	0.02	0.89	0.05
Gd	3.70	0.28	2.30	0.11	3.67	0.08	4.48	0.13	3.89	0.11	4.24	0.28
Tb	0.73	0.03	n.d.		0.78	0.03	0.93	0.03	n.d.		n.d.	
Dy	5.35	0.22	6.00	0.45	6.09	0.25	6.76	0.18	5.52	0.11	5.81	0.36
Ho	1.13	0.06	1.53	0.17	1.34	0.06	1.48	0.06	n.d.		n.d.	
Er	3.43	0.09	4.87	0.64	4.13	0.13	4.42	0.10	3.67	0.07	3.70	0.25
Tm	0.51	0.02	n.d.		0.57	0.03	0.65	0.02	n.d.		n.d.	
Yb	3.26	0.21	4.92	0.59	3.69	0.08	4.14	0.15	3.46	0.07	3.35	0.25
Lu	0.53	0.04	0.85	0.07	0.55	0.02	0.64	0.03	0.53	0.01	0.51	0.04
Hf	0.14	0.04	<0.15		0.085	0.013	0.17	0.02	0.19	0.02	0.20	0.02
Ta	<0.04		<0.08		<0.02		<0.01		<0.02		<0.02	
Th	<0.04		<0.03		<0.02		<0.01		<0.01		<0.01	
U	<0.03		<0.03		<0.02		<0.02		<0.01		<0.01	

Sample	**KEC 86-72B** Low jadeite		**K 91-4** Low jadeite		**K 91-22** Low jadeite		**KEC 81-3** High jadeite		**KEC 81-7** High jadeite		**KEC 81-8** High jadeite	
Spots	$n = 7$	1σ	$n = 7$	1σ	$n = 7$	1σ	$n = 7$	1σ	$n = 7$	1σ	$n = 7$	1σ
Sc	65.7	2.7	45.0	1.0	74.1	1.6	39.6	0.8	42.2	2.3	63.0	2.1
V	218	34	135	2	228	10	n.d.		136	3	252	13
Cr	395	23	395	7	325	8	n.d.		<18		319	15
Ni	<50		29.3	3.3	20.3	1.4	n.d.		14.6	3.8	11.2	1.7
Ga	n.d.		13.7	0.9	16.3	0.4	n.d.		n.d.		n.d.	
Rb	<1		<0.25		<0.62		<0.1				<0.2	
Sr	0.28	0.07	0.23	0.03	0.18	0.003	0.60	0.10	0.49	0.02	0.34	0.04
Y	34.0	1.3	30.4	1.4	36.6	2.4	15.0	0.6	33.6	0.8	25.4	1.2
Zr	8.34	0.66	7.85	0.67	8.48	1.18	10.9	0.6	40.0	1.3	4.83	0.17
Nb	<0.4		<0.09		<0.26		<0.1		<0.1		<0.03	
La	<0.2		<0.04		<0.06		0.06	0.01	0.078	0.014	0.003	—
Ce	0.18	0.02	0.12	0.06	0.14	0.04	0.67	0.04	0.83	0.11	0.13	0.01
Pr	n.d.		n.d.		n.d.		n.d.		0.32	0.02	0.12	0.01
Nd	1.64	0.19	1.56	0.07	1.44	0.12	2.74	0.13	3.36	0.16	1.62	0.08
Sm	2.08	0.10	2.60	0.38	1.89	0.24	1.89	0.13	2.64	0.22	1.40	0.11
Eu	1.00	0.09	1.30	0.12	0.94	0.06	0.90	0.04	1.14	0.06	0.63	0.04
Gd	4.40	0.24	5.36	0.47	4.10	0.34	3.13	0.19	4.77	0.20	2.43	0.11
Tb	n.d.		n.d.		n.d.		n.d.		0.95	0.07	0.50	0.02
Dy	5.88	0.43	6.59	0.33	6.73	0.67	3.34	0.12	6.34	0.27	4.07	0.20
Ho	n.d.		n.d.		n.d.		0.61	0.02	1.36	0.09	0.99	0.06
Er	3.79	0.13	3.63	0.23	4.56	0.36	1.67	0.15	3.94	0.22	3.29	0.22
Tm	n.d.		n.d.		n.d.		n.d.		0.56	0.01	0.51	0.03
Yd	3.80	0.22	3.40	0.20	4.44	0.25	1.41	0.08	3.55	0.10	3.50	0.26
Lu	0.55	0.05	0.49	0.03	0.70	0.05	0.21	0.02	0.55	0.02	0.56	0.03
Hf	0.20	0.11	0.21	0.06	0.18	0.01	0.23	0.02	0.73	0.05	0.076	0.008
Ta	<0.07		<0.03		<0.05		<0.03		<0.02		<0.01	
Th	<0.05		<0.03		<0.05		<0.04		<0.02		0.001	0.001
U	<0.05		<0.02		<0.02		<0.03		0.041	0.014	0.004	0.001

(Continued)

Table 3. (Continued)

Sample	KEC 81-10A High jadeite		KEC 81-21 High jadeite		K 91-11 High jadeite		K 91-58 High jadeite		KEC 86-KB-3 Kyanite-bearing		KEC 86-KB-4 Kyanite-bearing	
Spots	$n = 7$	1σ	$n = 7$	1σ	$n = 9$	1σ	$n = 7$	1σ	$n = 5$	1σ	$n = 8$	1σ
Sc	62.9	3.3	69.7	1.1	51.7	1.6	54.2	1.1	36.4	1.9	28.9	1.5
V	117	14	148	12	165	10	255	10	147	6	433.1	31.3
Cr	266	34	519	44	254	28	131	5	297	26	783.7	43.8
Ni	18.2	2.3	36.6	2.1	15.7	1.9	9.9	0.6	23.3	3.2	33.2	4.8
Ga	n.d.		n.d.		14.40	0.65	18.40	0.60	n.d.		n.d.	
Rb	<0.3		0.66	0.07	<1.05		<0.8		<0.6		<0.5	
Sr	0.50	0.03	0.41	0.03	0.33	0.03	0.58	0.07	2.28	0.14	1.66	0.07
Y	20.7	2.8	32.8	2.5	43.4	2.4	56.7	1.0	13.2	0.5	6.53	0.42
Zr	44.9	6.3	14.6	2.6	26.7	2.2	15.0	0.8	9.12	0.30	5.05	0.37
Nb	0.21	0.03	0.07	0.02	<0.23		<0.24		<0.2		<0.2	
La	0.019	0.002	0.009	0.001	<0.08		<0.08		<0.1		0.029	0.003
Ce	0.19	0.02	0.08	0.02	0.44	0.06	0.40	0.09	0.21	0.07	0.50	0.08
Pr	0.085	0.012	n.d.		n.d.		n.d.		n.d.		n.d.	
Nd	1.10	0.11	0.54	0.08	2.34	0.08	2.25	0.13	1.78	0.20	2.58	0.27
Sm	1.11	0.12	0.69	0.12	2.55	0.18	2.59	0.16	1.28	0.17	1.39	0.28
Eu	0.63	0.07	0.46	0.08	1.10	0.09	1.29	0.05	0.76	0.06	0.60	0.11
Gd	2.71	0.35	2.51	0.25	5.47	0.34	5.77	0.28	2.11	0.15	1.58	0.15
Tb	0.55	0.05	n.d.		n.d.		n.d.		n.d.		n.d.	
Dy	4.03	0.49	5.26	0.28	8.23	0.77	10.78	0.49	2.66	0.23	1.63	0.25
Ho	0.88	0.10	n.d.		n.d.		n.d.		n.d.		n.d.	
Er	2.63	0.27	4.29	0.26	5.65	0.53	7.25	0.27	1.60	0.20	0.79	0.10
Tm	0.41	0.03	n.d.		n.d.		n.d.		n.d.		n.d.	
Yb	2.80	0.16	4.71	0.26	5.48	0.52	6.70	0.15	1.44	0.11	0.69	0.14
Lu	0.44	0.03	0.72	0.05	0.80	0.09	1.01	0.06	0.19	0.02	0.11	0.04
Hf	0.83	0.15	0.29	0.06	0.51	0.12	0.40	0.07	0.24	—	0.15	0.06
Ta	0.022	0.007	0.004	0.002	<0.06		<0.06		<0.06		<0.02	
Th	0.004	0.001	0.003	0.002	<0.04		0.04	0.03	<0.05		<0.03	
U	0.010	0.001	0.003	0.001	<0.04		0.02	0.01	<0.08		0.018	0.005

Sample	KEC 86-KB-74B Kyanite-bearing		KEC 86-GB-12 Graphite-bearing		KEC 86-GB-70 Graphite-bearing	
Spots	$n = 7$	1σ	$n = 7$	1σ	$n = 7$	1σ
Sc	27.6	1.6	73.7	2.4	59.4	2.0
V	67.4	8.4	162	6	89.3	5.9
Cr	134	6	285	13	723	57
Ni	32.7	5.7	<25		33.0	—
Ga	9.91	0.33	10.7	0.5	10.3	0.8
Rb	<0.9		<0.7		<1	
Sr	0.48	0.15	0.54	0.05	0.25	—
Y	8.67	0.74	68.9	1.6	53.6	0.6
Zr	9.32	4.42	21.5	3.0	19.2	1.7
Nb	<0.4		<0.6		<0.9	
La	<0.05		<0.06		<0.08	
Ce	0.11	0.02	0.29	0.03	0.043	0.006
Pr	n.d.		n.d.		n.d.	
Nd	2.31	0.14	2.29	0.18	0.32	0.05
Sm	2.18	0.17	3.37	0.11	0.72	0.10
Eu	0.91	0.02	1.49	0.05	0.48	0.03
Gd	2.67	0.12	8.65	0.38	2.96	0.10
Tb	n.d.		n.d.		n.d.	
Dy	1.93	0.13	11.95	0.36	7.56	0.10
Ho	n.d.		n.d.		n.d.	
Er	0.74	0.08	7.15	0.18	7.18	0.15
Tm	n.d.		n.d.		n.d.	
Yb	0.55	0.04	6.39	0.13	8.24	0.26
Lu	0.08	0.01	0.98	0.02	1.38	0.04
Hf	0.17	0.06	0.39	0.06	0.35	0.06
Ta	<0.02		<0.03		<0.03	
Th	<0.01		<0.01		<0.02	
U	0.006	0.001	0.010	0.006	<0.01	

Concentrations are given in ppm (μg/g). Low jadeite = <30 mol.% jadeite in cpx. High jadeite = >30 mol.% jadeite in cpx. n. d. = not determined. Cs, Ba, and Pb were measured but below the detection limit in all samples analyzed. Typical detection limits are 0.2 ppm for Cs, 0.05 ppm for Ba, and 0.2 ppm for Pb (see Longerich et al. (1996) for definition of LA-ICP-MS detection limits).

calibrated against the silicate glass reference materials NIST 610 and NIST 612, and the USGS glass standards BCR-2g and BIR-1g were measured to monitor accuracy (Table 1).

4. RESULTS

4.1. Oxygen Isotopes

Garnet oxygen isotopic data were obtained for 31 low MgO eclogites (Table 2 and Fig. 1). Garnet is usually the freshest phase in eclogite xenoliths, is more resistant to isotopic resetting than clinopyroxene (Deines and Haggerty, 2000), and shows a larger range in composition (e.g., FeO content) than clinopyroxene (cpx). Garnet analyses are representative of the whole rock oxygen isotopic composition because the theoretical and observed high-temperature isotope fractionation between garnet and cpx is small (<0.4‰) (Rosenbaum and Mattey, 1995; Kohn and Valley, 1998; Snyder et al., 1998), with garnet generally being lighter than cpx.

Values of $\delta^{18}O$ in the Koidu eclogites range between 4.68 and 6.78‰ for garnet ($n = 31$, Fig. 1) between 5.12 and 5.73‰ for cpx ($n = 3$), and between 5.48 and 5.70‰ for kyanite ($n = 3$). Thus, neither very heavy nor very light values, as reported from South African eclogites (between 2.2 and 8.0‰, determined by conventional fluorination) (MacGregor and Manton, 1986) are observed.

Eighteen of the low MgO garnets lie within the mantle range (based on garnets from peridotites: $\delta^{18}O = 5.4 \pm 0.4$‰) (Mattey et al., 1994b), but 13 samples exceed the mantle range, being both isotopically lighter and heavier (Fig. 1). Values of $\delta^{18}O$ do not show a correlation with other elements (e.g., FeO, CaO) of garnet or whole rock, as reported for some Siberian eclogite xenoliths (Jacob et al., 1994; Jacob and Foley, 1999).

Three cpx and three kyanite separates were analyzed to determine the degree of oxygen isotopic equilibrium within the xenoliths. The observed isotope fractionation for the three kyanite-garnet pairs ranges between 0.35 and 0.59‰; fractionation for the three cpx-garnet pairs varies from −0.16 to 0.04‰. Values of $\Delta^{18}O_{ky\text{-}gt}$ are well within the range of isotope fractionations measured by laser fluorination in eclogite xenoliths from other locations (e.g., Mattey et al., 1994b), suggesting that the kyanite-garnet pairs are at (or at least close to) high-temperature isotopic equilibrium. Values of $\Delta^{18}O_{cpx\text{-}gt}$ are lower than the predicted values (0.1–0.4‰) (Rosenbaum and Mattey, 1995), but it remains unresolved if this difference indicates isotopic disequilibrium or is due to differences in crystal chemistry or analytical uncertainty. Deines and Haggerty (2000) suggested that metasomatic events just before (on the order of millions of years) the kimberlite eruption can lower the $\delta^{18}O$ of pyroxene without significantly affecting the isotope record of garnet. Moreover, garnet is easier to analyze by laser fluorination than cpx (Valley et al., 1995) and values of $\alpha(CO_2\text{-}H_2O)$ used by different laboratories vary by up to 0.4‰ (Valley et al., 1995), requiring corrections to compare data sets from different laboratories.

4.2. Trace Element Mineral Chemistry

The trace element compositions of minerals from 21 Koidu low MgO eclogites (including garnet, cpx plus rutile or ilmenite), determined by laser ablation ICP-MS, are presented in Tables 3, 4, and 5. Additional rutile analyses have been published in Rudnick et al. (2000). Trace element analyses of the high MgO eclogites will be presented in a companion paper. None of the samples analyzed for trace elements contain apatite or rutile exsolution lamellae (cf. Fung and Haggerty, 1995). All samples show variable degrees of modal metasomatism. Therefore, care was taken to perform analyses on crack-free, unaltered areas of the minerals. The combination of the high-quality optical imaging system of the Harvard laser ablation setup and the time-resolved analysis of the ablation signals ensures that altered and/or metasomatized parts of the silicate minerals were recognized and excluded from the average trace element analyses. Rutile typically shows oriented exsolution lamellae of ilmenite ± spinel at 90° angles, which were probably formed by unmixing related to cooling and/or changes in pressure (see Haggerty (1983), and references therein, for a discussion of the origins of ilmenite lamellae in rutile). Some rutiles show thin (several μm) ilmenite rims. Laser ablation analyses include exsolution lamellae but exclude ilmenite rims. Due to the limited grain size and the nearly opaque nature of rutile in the thick sections (~100 μm) analyzed, altered parts of the rutile grains could not always be avoided during analysis. However, these were easily distinguished by their high abundances of incompatible trace elements (e.g., Sr, Ba) and were excluded from the averages.

Garnets are light rare earth element (LREE)-depleted with chondrite-normalized La contents (La_N) from 0.01 to 0.25 (Fig. 2; in some samples La is below the detection limit). Most garnets have relatively flat heavy rare earth element (HREE) patterns, with $(Dy/Yb)_N$ from 0.58 to 2.2. In addition, all garnets have high HREE contents (Yb_N from 6.7–32), with the kyanite-bearing samples having the lowest and the graphite-bearing samples having the highest HREE contents. All garnets analyzed from kyanite-bearing samples have positive Eu anomalies (Eu/Eu* = 1.18–1.44) and those in graphite-bearing samples have negative Eu anomalies (Eu/Eu* = 0.82–0.90). All garnets show variable degrees of Zr, Hf, and Ti depletion (Fig. 3) except for two samples without primary rutile (KEC 81-10A and KEC 81-21). Garnets from samples with jadeite-poor (<30%) cpx have the strongest negative Zr, Hf, and Ti anomalies, while some of the garnets of the jadeite-rich eclogites have only slightly negative Zr and Hf anomalies. In the majority of garnets, Nb and Ta are below the detection limit (0.03–0.3 ppm and 0.01–0.08 ppm for Nb and Ta, respectively, depending on spot size). Nb and Ta depletions in garnet correlate with the presence of rutile. Samples KEC 81-10A and KEC 81-21 (without primary rutile) contain the highest concentrations of Nb and Ta. The concentration of alkali and alkaline earth elements in garnets are generally very low (e.g., 0.2–0.6 ppm Sr) or below the detection limits (e.g., Rb, Cs, Ba), but Sr ranges between 1.6 and 2.3 ppm in kyanite-bearing samples. Th and U concentrations are very low (3–41 ppb) or below the detection limits.

Clinopyroxenes have convex-upward REE patterns and are LREE-enriched relative to the HREE (Fig. 4). La_N contents range from 0.8 to 14 and Yb_N ranges from 0.15 to 1.1. Most clinopyroxenes show pronounced Nb and Ta depletions and variable degrees of Zr and Ti depletion (except that in samples KEC 81-10A and KEC 81-21, which lack primary rutile) (Fig. 5). The concentrations of Rb, Cs, and Ba are generally below

Table 4. Trace element composition of clinopyroxene determined by LA-ICP-MS.

Sample	KEC 80-A2 Low jadeite		KEC 81-4 Low jadeite		KEC 81-5 Low jadeite		KEC 81-18 Low jadeite		KEC 86-6 Low jadeite		KEC 86-56 Low jadeite	
Spots	$n = 10$	1σ	$n = 7$	1σ	$n = 7$	1σ	$n = 7$	1σ	$n = 7$	1σ	$n = 7$	1σ
Sc	28.0	2.0	32.9	0.8	32.4	1.3	30.7	0.4	30.1	2.0	28.2	1.3
V	492	13	n.d.		607	6	423	16	417	5	494	11
Cr	279	20	n.d.		706	21	248	17	253	5	313	7
Ni	355	35	n.d.		362	40	107	8	239	7	87.7	20.2
Ga	n.d.		n.d.		n.d.		n.d.		16.6	0.7	18.6	0.5
Rb	<0.4		<0.7		<0.3		<0.08		<0.5		<0.7	
Sr	85.7	4.6	70.7	4.3	147	6	116	3	80.6	1.5	144	2
Y	0.81	0.08	4.33	0.13	1.19	0.07	0.79	0.02	0.64	0.06	0.82	0.04
Zr	7.84	0.62	19.7	2.0	13.9	0.4	19.1	1.2	18.8	2.4	20.6	0.6
Nb	<0.1		<0.05		<0.08		<0.02		<0.5		<0.5	
Ba	<0.06		0.20	0.03	0.082	0.014	0.081	0.025	0.035	0.012	0.053	0.012
La	0.56	0.05	2.01	0.17	1.69	0.27	1.13	0.10	0.25	0.02	1.02	0.04
Ce	2.68	0.23	5.85	0.29	4.77	0.58	4.55	0.51	1.76	0.13	4.62	0.08
Pr	0.64	0.04	n.d.		1.00	0.08	0.86	0.07	n.d.		n.d.	
Nd	4.29	0.41	6.94	0.23	6.24	0.43	4.63	0.36	3.75	0.16	5.94	0.20
Sm	1.04	0.07	2.64	0.07	1.68	0.09	1.07	0.09	1.00	0.10	1.63	0.06
Eu	0.25	0.02	0.75	0.03	0.42	0.03	0.28	0.03	0.25	0.03	0.43	0.02
Gd	0.56	0.03	2.57	0.11	1.04	0.11	0.65	0.07	0.60	0.06	0.92	0.04
Tb	0.070	0.006	n.d.		0.11	0.01	0.068	0.007	n.d.		n.d.	
Dy	0.25	0.03	1.46	0.06	0.46	0.03	0.28	0.01	0.21	0.01	0.32	0.02
Ho	0.027	0.003	0.19	0.01	0.057	0.010	0.03	0.00	n.d.		n.d.	
Er	0.065	0.004	0.36	0.03	0.089	0.012	0.062	0.009	0.063	0.010	0.058	0.004
Tm	<0.02		n.d.		0.012	—	0.007	0.002	n.d.		n.d.	
Yb	0.02	—	0.13	0.01	0.050	0.002	0.035	0.004	0.031	0.004	0.035	0.002
Lu	<0.02		0.020	0.001	<0.02		0.004	0.000	<0.02		<0.01	
Hf	0.75	0.15	1.15	0.08	1.09	0.08	1.24	0.06	1.28	0.07	1.30	0.04
Ta	0.003	—	<0.02		<0.02		<0.01		<0.02		<0.02	
Pb	n.d.		n.d.		n.d.		n.d.		0.10	0.01	0.17	0.02
Th	0.042	0.015	0.082	0.008	0.14	0.02	0.035	0.005	0.009	0.002	0.018	0.005
U	0.005	0.001	0.018	0.002	0.019	0.002	0.015	0.004	<0.01		<0.01	

Sample	KEC 86-72B Low jadeite		K 91-4 Low jadeite		K 91-22 Low jadeite		KEC 81-3 High jadeite		KEC 81-7 High jadeite		KEC 81-8 High jadeite	
Spots	$n = 7$	1σ	$n = 7$	1σ	$n = 7$	1σ	$n = 7$	1σ	$n = 7$	1σ	$n = 7$	1σ
Sc	30.0	0.6	15.5	0.1	30.3	0.5	14.6	1.1	12.0	0.7	23.6	1.1
V	381	29	396	6	531	7.38	n.d.		368	4	534	29
Cr	262	47	375	7	221	8.81	n.d.		1470	596	251	17
Ni	66.4	5.9	468	17	399	11	n.d.		168	5	246	25
Ga	n.d.		21.7	0.6	19.2	0.4	n.d.		n.d.		n.d.	
Rb	<0.4		<0.67		0.60	0.07	<0.1		<0.4		<0.1	
Sr	150	10	102	4	66.8	6.8	145	5	108	2	143	13
Y	1.18	0.04	0.98	0.10	0.80	0.06	0.23	0.04	1.12	0.03	0.60	0.02
Zr	26.3	0.8	9.94	0.66	10.5	3.2	15.2	1.0	28.9	0.8	5.74	0.19
Nb	<0.2		<0.4		<0.16		<0.1		<0.1		<0.03	
Ba	0.066	0.004	0.10		0.05	0.00	0.15	0.06	0.38	0.03	0.048	0.017
La	1.49	0.06	0.30	0.02	0.73	0.06	2.11	0.09	4.35	0.20	1.15	0.17
Ce	5.96	0.18	2.16	0.11	3.17	0.20	8.29	0.33	13.07	0.31	4.24	0.52
Pr	n.d.		n.d.		n.d.		n.d.		1.84	0.06	0.75	0.07
Nd	5.64	0.20	5.43	0.33	4.02	0.19	5.92	0.33	8.30	0.21	3.74	0.29
Sm	1.39	0.10	1.90	0.23	1.02	0.06	0.96	0.17	1.55	0.10	0.74	0.06
Eu	0.38	0.02	0.46	0.04	0.27	0.02	0.23	0.03	0.36	0.02	0.19	0.01
Gd	0.95	0.06	1.17	0.11	0.74	0.10	0.45	0.05	0.93	0.09	0.42	0.03
Tb	n.d.		n.d.		n.d.		n.d.		0.94	0.008	0.045	0.004
Dy	0.41	0.02	0.35	0.04	0.30	0.06	0.14	0.02	0.39	0.04	0.20	0.01
Ho	n.d.		n.d.		n.d.		<0.03		0.55	0.005	0.028	0.004
Er	0.10	0.01	<0.2		0.09	0.01	<0.09		0.10	0.01	0.057	0.006
Tm	n.d.		n.d.		n.d.		n.d.		<0.02		0.007	0.001
Yb	0.037	0.006	<0.15		<0.08		<0.09		0.046	0.009	0.032	0.002
Lu	<0.03		<0.06		<0.03		<0.03		<0.02		0.004	0.001
Hf	1.42	0.17	0.81	0.11	1.03	0.17	0.98	0.06	1.82	0.10	0.44	0.05
Ta	<0.03		<0.07		<0.03		<0.03		<0.02		<0.01	
Pb	0.25	0.03	0.26	0.04	0.22	0.02	n.d.		n.d.		n.d.	
Th	0.037	0.010	<0.06		0.050	0.009	0.078	0.014	0.032	0.004	0.050	0.009
U	0.011	0.003	<0.04		<0.02		0.036	0.003	0.023	0.002	0.022	0.004

Concentrations are given in ppm (μg/g). Low jadeite = <30 mol.% jadeite in cpx. High jadeite = >30 mol.% jadeite in cpx. n. d. = not determined. Cs, was measured but below the detection limit in all samples analyzed.

Table 4. (Continued)

Sample	KEC 81-10A High jadeite		KEC 81-21 High jadeite		K 91-11 High jadeite		K 91-58 High jadeite		KEC 86-KB-3 Kyanite-bearing		KEC 86-GB-12 Graphite-bearing	
Spots	$n = 7$	1σ	$n = 7$	1σ	$n = 7$	1σ	$n = 6$	1σ	$n = 6$	1σ	$n = 7$	1 σ
Sc	12.0	0.5	19.7	0.3	23.4	0.4	26.0	0.8	14.4	0.5	25.2	1.5
V	335	18	373	19	397	2	538	13	202	6	424	4
Cr	270	24	479	11	222	21	94	7	184	13	264	4
Ni	132	24	350	7	237	5	110	4	360	7	123	7
Ga	n.d.		n.d.		17.8	0.4	26.5	0.6	n.d.		17.5	0.5
Rb	<0.1		0.36	0.08	1.08	0.07	0.90	0.09	<0.6		<0.6	
Sr	61	2	119	9	130	3	99	6	68.5	48.5	158	3
Y	0.72	0.07	1.27	0.07	2.02	0.06	1.10	0.10	0.10	0.03	1.43	0.09
Zr	20.1	2.6	11.1	3.05	35.5	0.7	22.6	2.5	8.52	1.47	32.9	2.5
Nb	0.16	0.02	0.12	0.03	<0.11		<0.16		<0.2		<0.5	
Ba	0.041	0.008	0.61	0.013	2.08	0.23	0.066	0.015	<0.1		0.63	0.04
La	0.33	0.04	0.45	0.02	3.98	0.14	0.61	0.06	<0.1		1.06	0.06
Ce	1.39	0.11	1.85	0.11	12.5	0.3	2.07	0.23	0.051	0.023	4.18	0.19
Pr	0.26	0.02	n.d.		n.d.		n.d.		n.d.		n.d.	
Nd	1.58	0.10	1.70	0.13	9.08	0.41	2.21	0.08	0.54	0.17	5.24	0.31
Sm	0.45	0.04	0.51	0.05	2.16	0.17	0.79	0.08	0.22	0.02	1.60	0.09
Eu	0.15	0.01	0.17	0.02	0.56	0.05	0.25	0.02	0.06	0.01	0.41	0.03
Gd	0.39	0.06	0.48	0.05	1.46	0.13	0.69	0.13	0.19	0.01	1.21	0.05
Tb	0.045	0.005	n.d.		n.d.		n.d.		n.d.		n.d.	
Dy	0.23	0.05	0.33	0.05	0.66	0.07	0.39	0.04	<0.3		0.44	0.05
Ho	0.028	0.005	n.d.		n.d.		n.d.		n.d.		n.d.	
Er	0.056	0.006	0.11	0.02	0.19	0.02	0.12	0.03	<0.2		0.097	0.011
Tm	0.006	0.001	n.d.		n.d.		n.d.		n.d.		n.d.	
Yb	0.037	0.013	0.067	0.014	0.082	0.002	0.083	0.011	<0.16		0.052	0.011
Lu	0.004	0.001	0.010	0.004	<0.02		<0.03		<0.05		<0.02	
Hf	1.40	0.25	0.64	0.11	2.14	0.14	1.89	0.12	0.73	0.12	1.99	0.16
Ta	0.023	0.008	0.009	0.003	<0.30		<0.05		<0.06		<0.02	
Pb	n.d.		0.24	0.03	1.24	0.12	0.37	0.06	n.d.		0.47	0.03
Th	0.004	0.001	0.008	0.002	0.12	0.02	<0.03		<0.07		<0.01	
U	0.003	0.001	<0.01		<0.03		<0.01		<0.04		<0.01	

(Continued)

Sample	KEC 86-GB-70 Graphite-bearing	
Spots	$n = 7$	1σ
Sc	23.0	1.4
V	271	3
Cr	703	14
Ni	243	12
Ga	14.1	0.5
Rb	<0.8	
Sr	154	3
Y	4.36	0.13
Zr	39.9	1.2
Nb	<0.7	
Ba	1.51	0.12
La	2.39	0.10
Ce	5.24	0.24
Pr	n.d.	
Nd	4.68	0.27
Sm	1.65	0.10
Eu	0.56	0.03
Gd	1.76	0.07
Tb	n.d.	
Dy	1.24	0.06
Ho	n.d.	
Er	0.393	0.033
Tm	n.d.	
Yb	0.221	0.023
Lu	0.033	0.005
Hf	2.28	0.11
Ta	<0.02	
Pb	0.76	0.03
Th	0.054	0.008
U	0.008	0.001

the detection limit. Cpx in only one of the kyanite-bearing eclogites (KEC 86-KB-3) was measured because cpx in the other kyanite-bearing samples was pervasively altered to white, fine-grained aggregates.

Rutiles in the low MgO eclogites have highly variable concentrations of Nb and Ta, with Nb/Ta ranging from subchondritic to superchondritic (Table 5) (Rudnick et al., 2000). The rutiles have high and relatively homogeneous W, Mo, Zr, Hf, Sn, and V contents and REE and Sb contents below the detection limit. Secondary (metasomatic) rutile in KEC 81-10A and KEC 81-21 is distinguished by much higher and heterogeneous Nb and Ta contents (16,000 ppm Nb and 900–1700 ppm Ta) and occasionally by a skeletal texture. Secondary rutile with much higher Nb contents than primary rutile has also been reported for eclogite xenoliths from the Kasai-Congo craton (El Fadili and Demaiffe, 1999). Ilmenite in sample K91-58, the sole ilmenite-bearing low MgO eclogite analyzed, has trace element contents similar to rutile but lower Zr and Hf and higher Ni concentrations.

Trace element contents of kyanite are below detection limits, except for V, Cr, and Ga. However, due to the lack of an appropriate internal standard (counting rates for both Al and ^{29}Si were above the pulse-counting threshold), absolute concentrations could not be calculated.

4.3. Clinopyroxene/Garnet Trace Element Partitioning

Both the absolute trace element concentrations and the cpx/garnet partition coefficients ($D^{cpx/gt}$) of the samples analyzed in

Table 5. Trace element composition of rutile determined by LA-ICP-MS.

Sample	**K91-4**		**K91-22**		**K91-11**		**K91-58**	
Mineral	Low jadeite rutile		Low jadeite rutile		High jadeite rutile		High jadeite ilmenite	
spots	$n = 10$	1σ	$n = 7$	1σ	$n = 7$	1σ	$n = 10$	1σ
Sc	3.12		5.43	0.80	<4.5		6.62	0.26
V	1995	92	2400	42	1283	41	1535	89
Cr	1272	108	716	43	509	28	178	41
MnO wt.%	0.020	0.011	0.020	0.010	0.008	0.007	0.32	0.05
FeO wt.%	2.43	0.38	2.89	0.57	3.63	0.80	31.5	2.8
Ni	<50		26.1		39.4	9.0	105	14
Zn	27.2	10.5	20.7	2.6	44.3	17.4	414	102
Zr	636	70	548	24	1653	111	233	24
Nb	69.9	1.2	83.0	5.2	1060	9	1785	93
Mo	<8		6.13	1.03	8.16	1.75	<4	
Sn	49.5	7.9	31.1	1.9	37.4	3.3	5.01	0.48
Sb	<1.6		<0.9		<1		<0.7	
Hf	18.8	3.2	25.3	3.6	39.6	4.9	4.73	1.34
Ta	8.58	0.29	2.55	1.42	8.18	0.31	79.4	16.8
W	3.24	0.76	8.38	3.88	14.86	0.80	0.83	0.47
Pb	<0.5		<0.3		<0.3		0.28	0.03
Th	<0.2		<0.1		<0.1		<0.1	
U	0.66	0.03	3.15	0.59	3.36	0.17	<0.1	

Concentrations are given in ppm (μg/g). Low jadeite = < 30 mol.% jadeite in cpx. High jadeite = > 30 mol.% jadeite in cpx. n. d. = not ppm determined. Rb, Sr, Y, and REE were measured but below the detection limit in all samples analyzed. Additional data given in Rudnick et al. (2000).

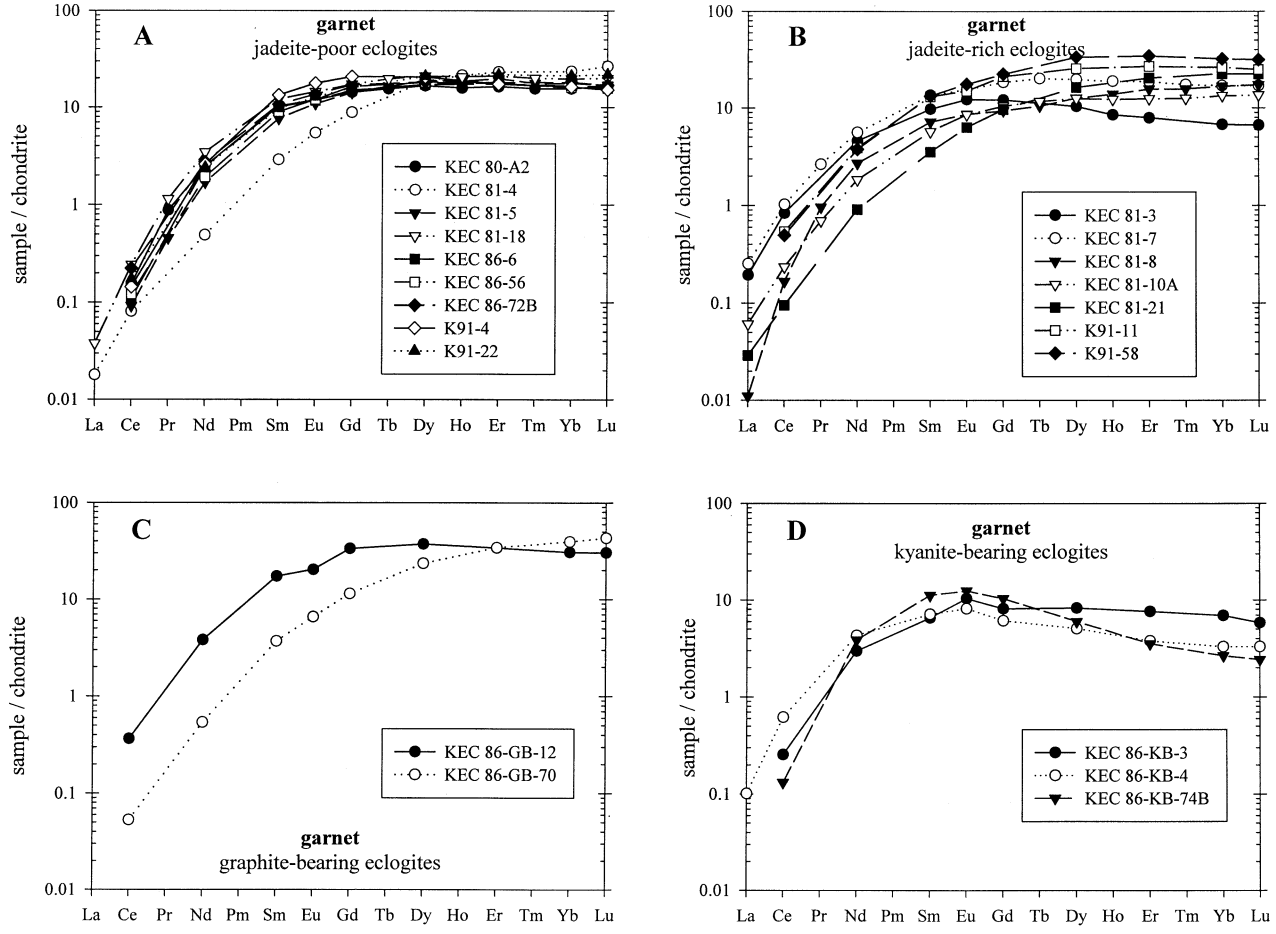

Fig. 2. Chondrite-normalized garnet REE data for Koidu low MgO eclogite xenoliths. (A) Jadeite-poor eclogites (<30 mol.% jadeite in cpx). (B) Jadeite-rich eclogites (>30 mol.% jadeite in cpx). (C) Graphite-bearing eclogites. (D) Kyanite-bearing eclogites. Element abundances are normalized to the chondrite values of Boynton (1984).

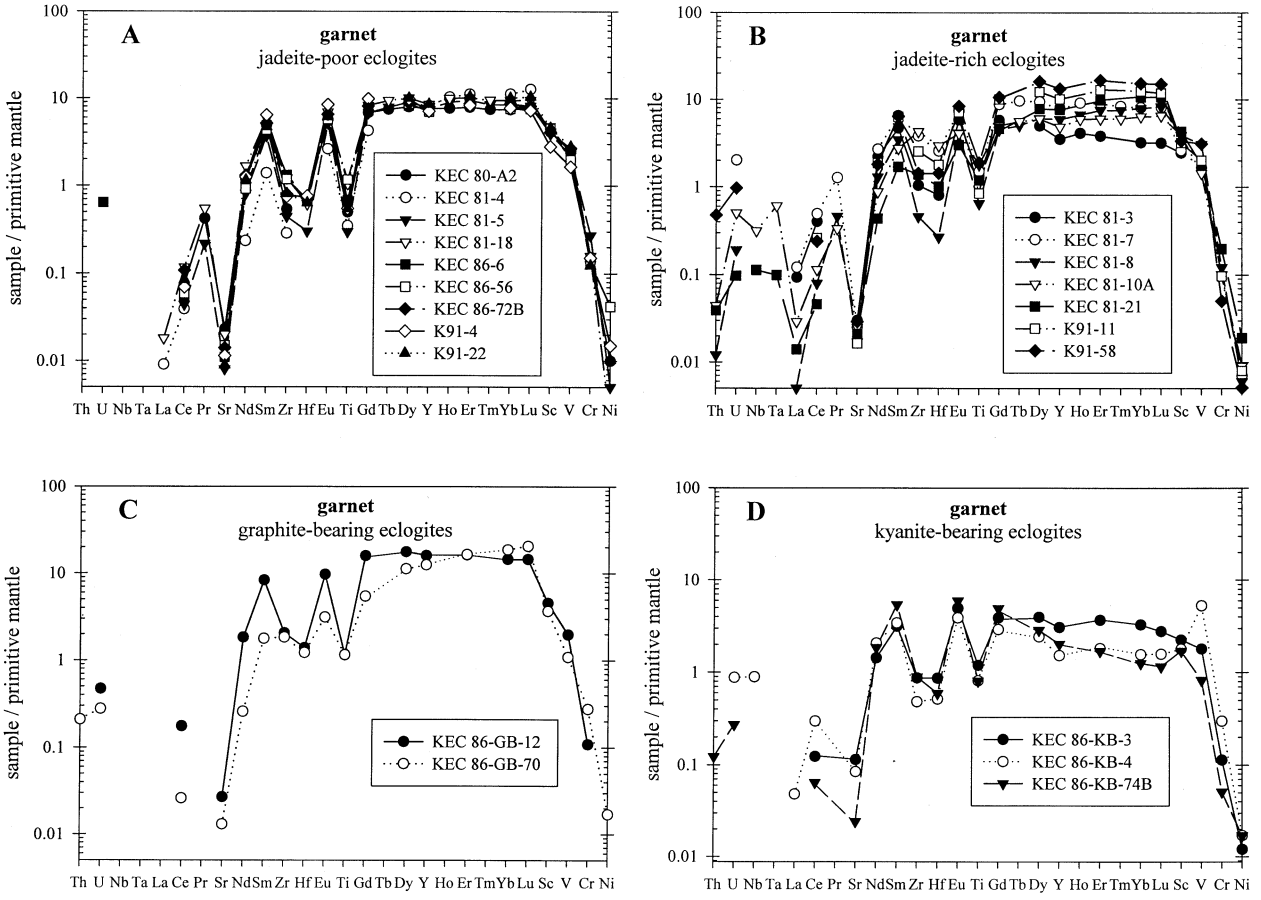

Fig. 3. Mantle-normalized garnet trace element diagrams for Koidu low MgO eclogite xenoliths. (A) Jadeite-poor eclogites (<30 mol.% jadeite in cpx). (B) Jadeite-rich eclogites (>30 mol.% jadeite in cpx). (C) Graphite-bearing eclogites. (D) Kyanite-bearing eclogites. Element abundances are normalized to the primitive mantle values of McDonough and Sun (1995).

our study show a wide range of values. $D^{cpx/gt}$ for the Koidu eclogite suite varies by two orders of magnitude for highly incompatible elements such as LREE and Sr but the variation is less with decreasing incompatibility. Such systematics are typical for high-temperature equilibrium trace element partitioning in eclogite xenolith suites (Harte and Kirkley, 1997) and indicate that the Koidu eclogites were at or close to trace element equilibrium at the time of their entrainment into the kimberlite. The changes in $D^{cpx/gt}$ for trace elements are correlated with Ca/(Ca + Mg) or Ca/(R^{2+}), where R^{2+} refers to all divalent cations, in garnet and cpx, such that $D^{cpx/gt}$ decrease as the Ca/(R^{2+} increase (Harte and Kirkley, 1997). In particular, $D^{cpx/gt}$ for trace elements show good correlations with the molar Ca partition coefficient (D_{Ca*}), which reflects a major compositional variable of the cpx and garnets (Fig. 6) (Harte and Kirkley, 1997). D_{Ca*} vs. $D^{cpx/gt}$ for compatible elements, e.g., Y (with respect to garnet and cpx), show good agreement with the trends established by Harte and Kirkley (1997) for the Roberts Victor eclogites (dashed lines in Fig. 6). The Koidu eclogites, however, have higher $D^{cpx/gt}$ for incompatible trace elements (e.g., Sr, Nd), especially in Ca-rich samples. This discrepancy can be explained, at least in part, by the temperature difference between the Roberts Victor eclogite suite and the Koidu suite. Based on the lattice-strain model (Blundy and Wood, 1994; Wood and Blundy, 1997), one would expect greater fractionation of incompatible elements at lower equilibration temperatures. The lower average equilibration temperature of the Koidu low MgO eclogites (880–930°C) (Fung and Haggerty, 1995) compared with the samples of the Roberts Victor suite (~1100°C at 5 GPa) (Harte and Kirkley, 1997) may result in the observed higher $D^{cpx/gt}$.

4.4. Whole Rock Chemistry

Trace element compositions of 16 Koidu low MgO eclogite whole rock powders were determined by solution ICP-MS (Table 6; Fig. 7). All samples show variable enrichments in incompatible trace elements and flat HREE patterns (except KEC 86-74B, which is HREE depleted). Many samples have pronounced positive Nb anomalies and low Ti concentrations relative to REE. Some samples show negative Zr and Hf anomalies (e.g., KEC 81-5).

The whole rock analyses of these kimberlite-borne eclogite xenoliths are invariably enriched in incompatible trace elements relative to the compositions determined from the primary minerals alone (Fig. 8). Highly incompatible elements are

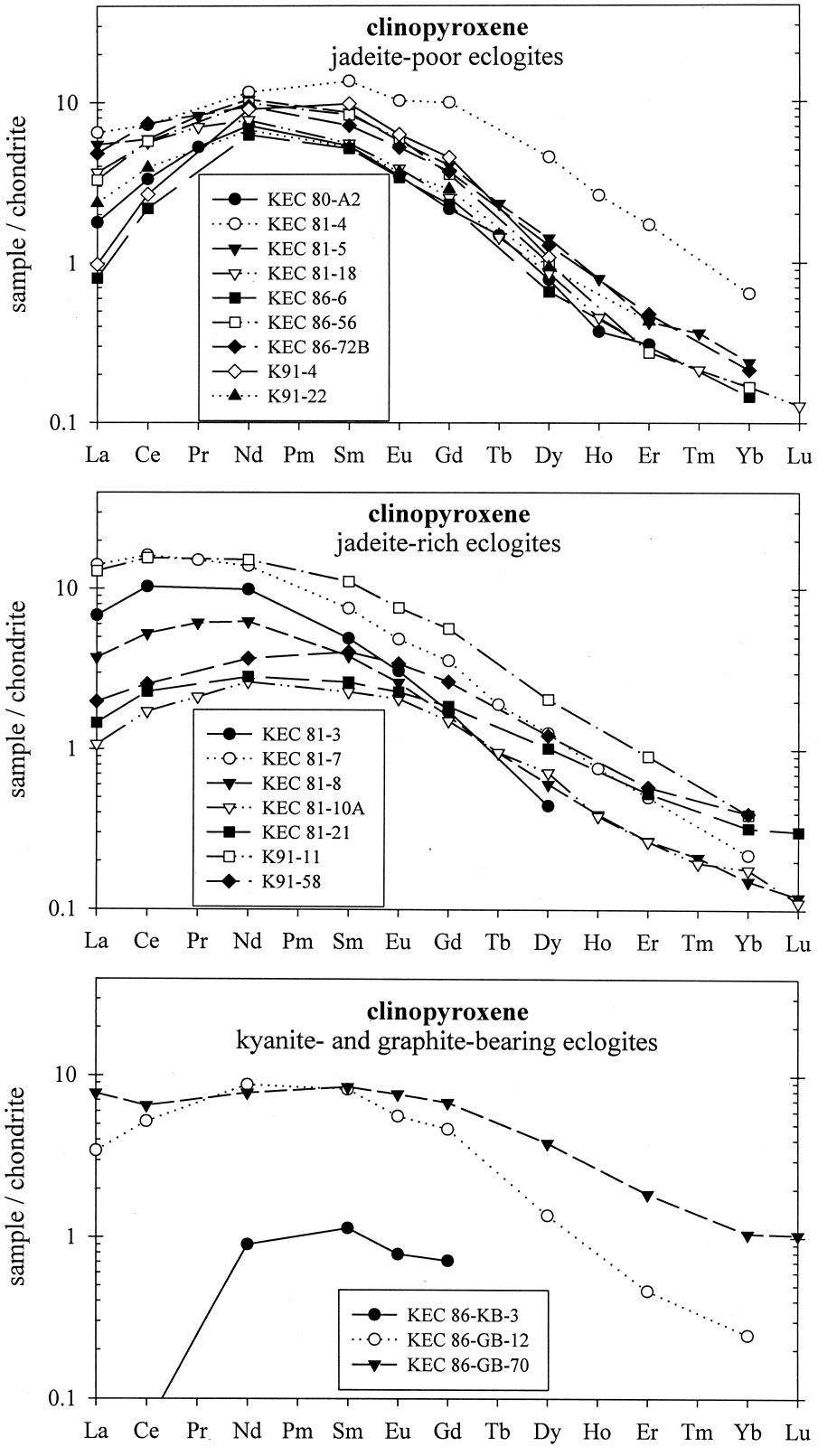

Fig. 4. Chondrite-normalized clinopyroxene REE data for Koidu low MgO eclogite xenoliths. Top: jadeite-poor eclogites (<30 mol.% jadeite in cpx). Middle: jadeite-rich eclogites (>30 mol.% jadeite in cpx). Bottom: kyanite- and graphite-bearing eclogites. Normalized as in Figure 2.

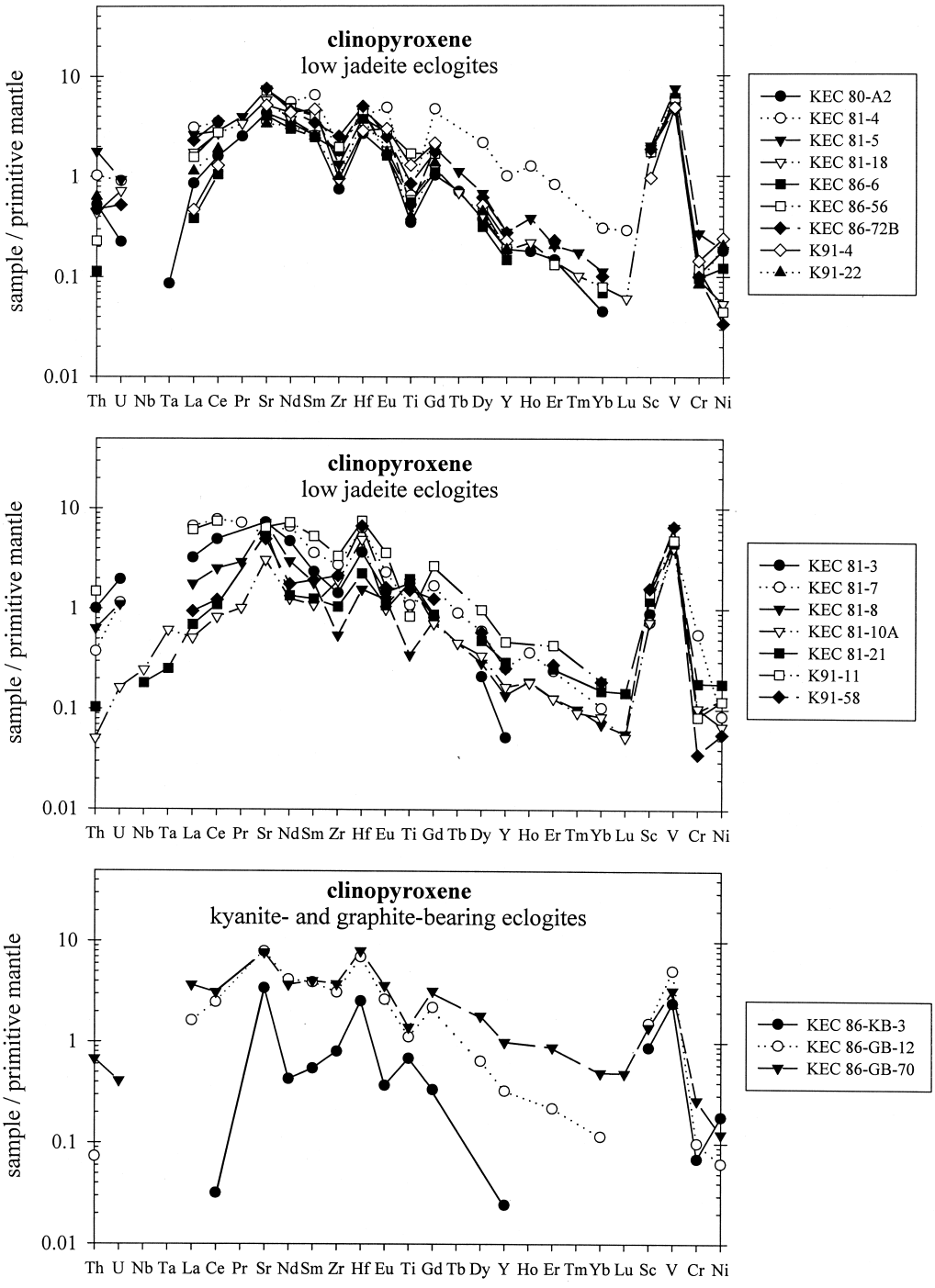

Fig. 5. Mantle-normalized clinopyroxene trace element diagrams for Koidu low MgO eclogite xenoliths. Top: jadeite-poor eclogites (<30 mol.% jadeite in cpx). Middle: jadeite-rich eclogites (>30 mol.% jadeite in cpx). Bottom: kyanite- and graphite-bearing eclogites. Normalized as in Figure 3.

affected more than moderately incompatible and compatible elements; for example, La shows high and variable enrichments in the analyzed whole rock while Yb is little affected by alteration. Except for rutile, accessory phases (e.g., apatite, zircon) can be ruled out as important hosts of trace elements because these phases are not observed in the samples.

In addition to the incompatible trace elements, some major elements appear to have been added to the xenoliths, as the measured whole rock compositions have higher concentrations than any of the extant primary phases. This is clearly the case for MgO, where some eclogite xenoliths have higher MgO contents in the whole rock than either garnet or cpx (see Fig. 12 in Fung and Haggerty, 1995). Thus, inexact modal estimates or small analytical uncertainties alone cannot explain the devia-

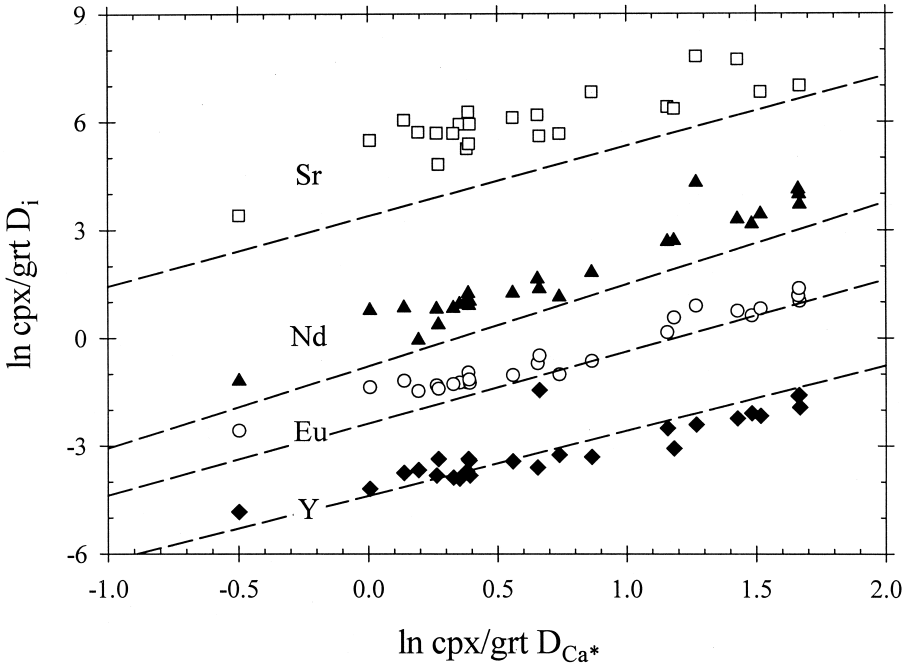

Fig. 6. Natural logarithms of clinopyroxene/garnet partition coefficients, ln D_i (ppm in cpx/ppm in gt), for Sr, Nd, Eu, and Y plotted against natural logarithms of molar partition coefficients for the major cation Ca, ln D_{Ca*}. Data from the present paper and Barth et al. (in prep). Dashed lines are the regression lines of Harte and Kirkley (1997) of an eclogite suite from Roberts Victor, South Africa.

tions between measured and reconstructed whole rock composition. Geological processes that may have contributed to these discrepancies include (1) metasomatism of eclogite in the mantle by passing silicate or carbonate magmas, (2) alteration and development of secondary phases associated with the host kimberlite (either before or during entrainment), and (3) weathering and interaction with groundwater that reacts with and percolates through the kimberlite and entrained xenoliths.

The high concentrations of incompatible trace elements and MgO in the kimberlite would result in a significant increase of these elements in xenoliths that were infiltrated by kimberlitic melts without significantly affecting other major elements or HREE. Infiltration and alteration by the host kimberlite is manifested by the presence of secondary phlogopite and amphibole in veins and along grain boundaries, which may be up to 20 modal % in some samples (Hills and Haggerty, 1989). Correlations between primary and secondary phase compositions indicate that the eclogitic minerals have been directly involved in the generation of the secondary phases (McCormick et al., 1994). That is, the secondary phases are probably products of kimberlitic melts reacting with primary garnet and clinopyroxene. The secondary phases are generally a lower pressure assemblage than the primary phases, suggesting that these phases crystallized en route to the surface in the kimberlite pipe (McCormick et al., 1994).

To evaluate this process quantitatively, we have performed mixing calculations between the host kimberlite (Taylor et al., 1994) and the reconstructed eclogites. For many samples, the differences between measured and reconstructed whole rock composition can be explained by addition of variable amounts of kimberlite. For example, the addition of ~5 wt.% kimberlite to the reconstructed whole rock composition of KEC 81-7 yields a reasonable approximation to the measured trace element composition (Fig. 8). However, higher amounts of kimberlite addition (~10%) are required to replicate the measured MgO content. Large variations in the relative fractionation of Nb and U, very high Nb contents in some samples (e.g., KEC 81-3 and KEC 86-13), and the occurrence of secondary rutile require at least one additional metasomatic process in these samples. Because several processes may be overprinted in these rocks, it is particularly difficult to constrain the nature of metasomatic processes other than kimberlite infiltration.

4.5. Whole Rock Reconstruction

To evaluate the chemical composition of the eclogites before their entrainment in the kimberlite, whole rock trace element patterns have been reconstructed based on the trace element contents measured in primary garnet, cpx, and oxides using previously published modal abundances (Table 7) (Hills and Haggerty, 1989; Fung and Haggerty, 1995) and Ti mass balance (see below).

The overall REE patterns of eclogite xenoliths are fairly insensitive to uncertainties in the proportions of garnet and cpx (Jerde et al., 1993). All eclogites have relatively flat HREE (Fig. 9). The jadeite-poor eclogites have very homogeneous LREE-depleted patterns, whereas the jadeite-rich eclogites have more variable LREE-depleted patterns. Samples KEC 81-3, KEC 81-10A, and KEC 86-KB-3 have positive Eu anomalies, and samples KEC 86-GB-12 and K91-11 have small negative Eu anomalies. Note that REE could only be reconstructed for one kyanite-bearing sample due to the low concen-

Table 6. Whole rock compositions of the Koidu low MgO eclogites measured by solution ICP-MS.

	KEC-81-3	KEC-81-4	KEC-81-5	KEC-81-7	KEC-81-8	KEC-81-10A	KEC-81-12	KEC-81-18
Ga	15.3	11.6	12.0	12.0	13.3	10.6	14.4	10.7
Rb	5.66	3.18	12.6	9.77	24.9	21.0	12.0	28.3
Sr	451	63.8	49.6	107	152	201	134	113
Y	13.9	22.8	24.5	24.0	18.3	9.47	42.1	17.3
Zr	32.0	26.1	17.3	80.4	30.6	46.5	58.6	53.6
Nb	16.1	5.16	9.10	25.6	15.9	16.0	6.53	15.4
Cs	0.11	0.03	0.31	0.10	1.12	0.12	0.40	0.30
Ba	1001	60.4	93.7	149	240	347	328	384
La	8.17	5.19	2.70	9.28	6.91	11.4	6.17	7.49
Ce	18.0	11.7	5.84	21.0	13.9	20.5	18.4	16.2
Pr	2.35	1.56	0.78	2.65	1.70	2.24	2.94	2.21
Nd	10.4	7.23	3.82	11.4	7.47	8.20	14.6	9.07
Sm	2.87	2.13	1.71	2.99	1.83	1.45	4.59	2.24
Eu	1.13	0.75	0.66	1.08	0.68	0.55	1.31	0.77
Gd	3.41	2.98	2.72	3.86	2.17	1.78	5.84	2.57
Tb	0.51	0.55	0.57	0.68	0.39	0.30	1.11	0.46
Dy	2.76	3.83	4.10	4.18	2.81	1.72	7.01	2.93
Ho	0.54	0.90	0.96	0.89	0.70	0.37	1.52	0.68
Er	1.36	2.65	2.76	2.49	2.18	1.01	4.37	1.90
Yb	11.1	2.51	2.42	2.21	2.32	0.88	4.08	1.90
Lu	0.16	0.39	0.36	0.34	0.36	0.14	0.62	0.28
Hf	1.00	1.00	0.64	2.36	1.08	1.43	1.77	1.72
Th	0.61	0.71	0.43	1.08	0.77	1.32	0.38	0.87
U	0.21	0.34	0.13	0.45	0.30	0.33	0.14	1.46

	KEC-81-21	KEC-81-DB-1	KEC-86-13	KEC-86-71A	KEC-86-71B	KEC-86-72A	KEC-86-72B	KEC-86-74B
Ga	11.5	12.4	11.3	11.7	11.7	13.5	13.2	16.3
Rb	8.17	12.6	11.9	13.3	14.8	17.6	8.78	21.6
Sr	104	89.3	136	108	163	187	116	372
Y	15.8	18.7	28.9	24.3	24.0	42.0	25.4	4.67
Zr	29.9	47.1	43.7	41.7	53.3	50.8	36.6	38.7
Nb	47.2	11.1	209	17.9	27.6	28.8	60.2	11.0
Cs	2.93	1.29	0.07	0.92	0.09	4.34	2.42	3.12
Ba	93.8	177	387	769	762	246	79.6	234
La	5.73	4.85	8.41	10.0	8.21	4.71	3.67	4.12
Ce	11.9	10.7	20.2	19.9	16.2	9.77	9.28	7.62
Pr	1.38	1.41	2.73	2.37	1.96	1.26	1.39	0.91
Nd	5.26	6.45	11.5	9.39	8.27	5.82	6.62	4.00
Sm	1.14	1.94	3.08	2.57	2.49	2.54	2.38	1.35
Eu	0.42	0.72	1.16	1.01	1.04	1.11	0.88	0.54
Gd	1.57	2.93	4.35	3.10	3.22	4.61	3.52	1.61
Tb	0.32	0.49	0.77	0.55	0.55	0.86	0.60	0.20
Dy	2.25	3.12	4.83	3.70	3.68	6.00	3.98	1.03
Ho	0.57	0.71	1.09	0.83	0.84	1.43	0.87	0.15
Er	1.84	2.03	2.99	2.57	2.32	4.19	2.52	0.36
Yb	1.94	1.83	2.77	2.41	2.18	4.01	2.30	0.27
Lu	0.32	0.28	0.42	0.36	0.33	0.63	0.34	0.03
Hf	0.97	1.31	1.00	0.89	1.17	1.60	1.23	1.00
Th	0.75	0.73	1.03	2.96	11.0	0.64	0.35	0.65
U	0.18	0.19	0.70	0.56	0.61	0.19	0.12	0.16

Concentrations are given in ppm (μg/g).

trations in the clinopyroxenes. However, small positive Eu anomalies in garnets from the three kyanite-eclogites (Fig. 2d) suggest that positive Eu anomalies are ubiquitous features of these rocks.

Some trace elements, such as the HFSE (high field-strength elements Ti, Zr, Hf, Nb, and Ta) may be largely contained in accessory phases such as rutile. This presents a problem for whole rock reconstructions as it is generally difficult to determine precise modal proportions of accessory phases by point counting coarse-grained rocks like eclogites. For this reason, we have calculated the modal abundance of rutile from Ti mass balance between the measured whole rock and mineral compositions (Rudnick et al., 2000). Proportions and Ti concentrations of garnet and cpx (Hills and Haggerty, 1989; Fung and Haggerty, 1995) were used to calculate the Ti content of the silicate fraction. This is invariably less than the measured whole rock. The missing Ti is assigned to rutile and the modal proportion is thus calculated. This method yields the maximum amount of rutile or ilmenite in the sample, since it does not account for any Ti in secondary phases such as metasomatic rutile, amphibole (0.5–2.5 wt.% TiO_2), or phlogopite (1.6–4 wt.% TiO_2). However, only one sample analyzed (KEC 81-18)

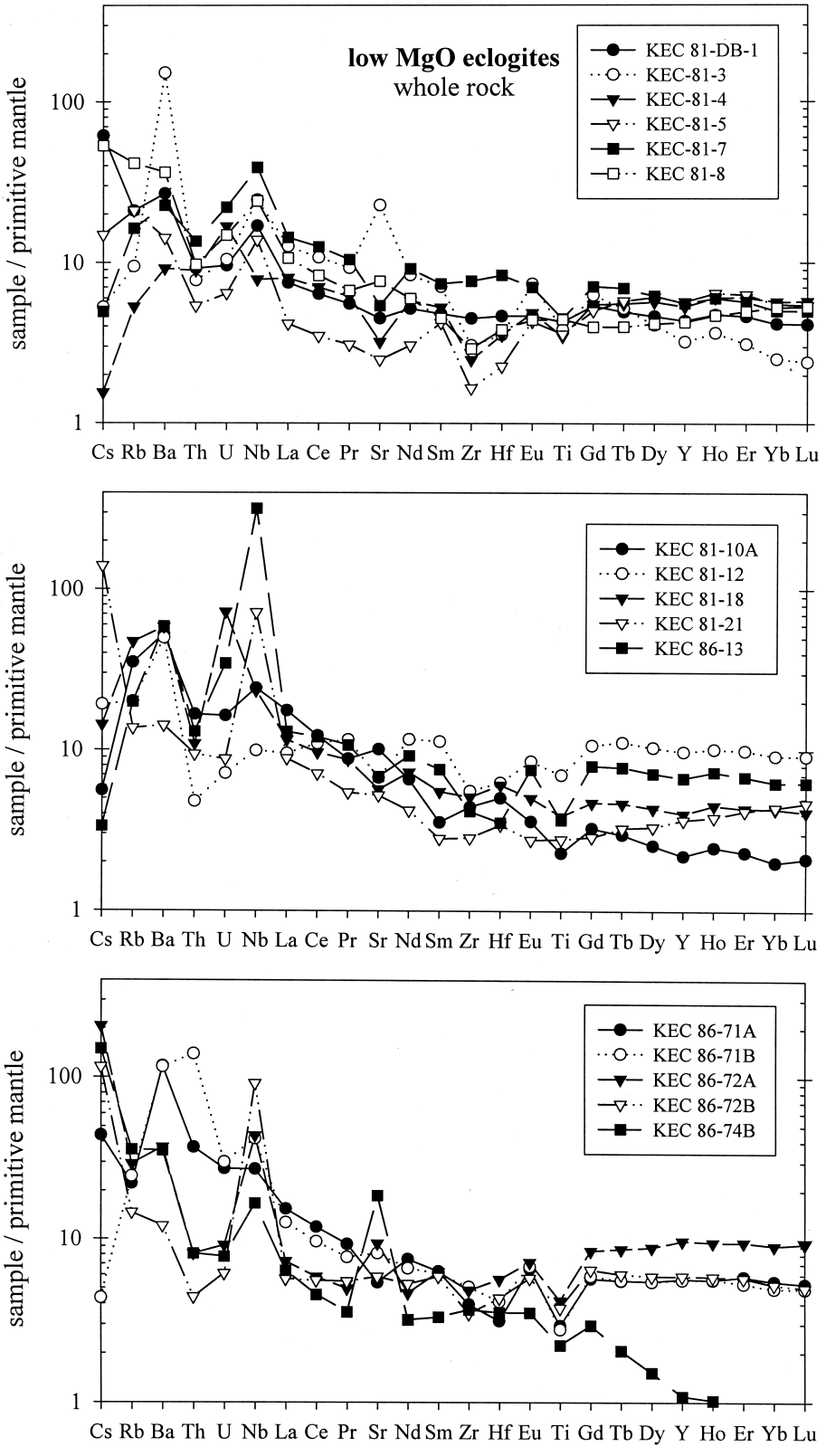

Fig. 7. Mantle-normalized whole rock trace element diagrams for Koidu low MgO eclogite xenoliths. Samples are sorted by number. Normalized as in Figure 3.

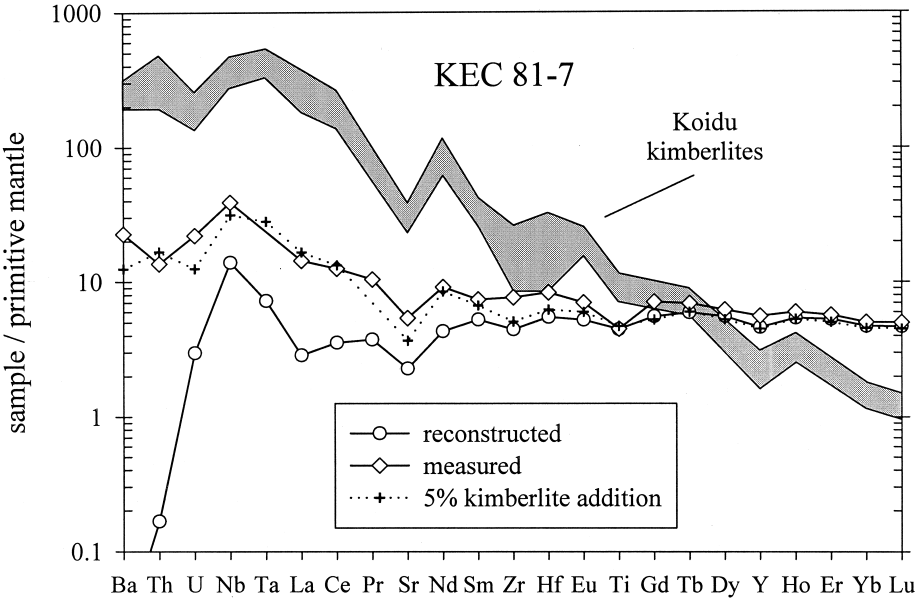

Fig. 8. Mantle-normalized trace element diagram illustrating kimberlite contamination. Gray field shows the range of kimberlite compositions at Koidu, Sierra Leone (Taylor et al., 1994). Open circles denote the reconstructed whole rock composition of sample KEC 81-7; open diamonds denote the measured whole rock composition. Crosses show calculated mixture of the reconstructed eclogite with 5% average Koidu kimberlite added. Normalized as in Figure 3.

contains two generations of rutile (KEC 81-10A and KEC 81-21 contain metasomatic rutile but no primary rutile). Therefore, any overestimation is small and within the errors of the estimated absolute uncertainty (±0.05%) (Rudnick et al., 2000). The reconstructed Nb concentration never exceeds the measured Nb concentration, suggesting that overestimation of the amount of rutile is not a problem. For samples lacking bulk rock TiO_2 concentrations, modal rutile was calculated by assuming that the bulk rock has no Ti anomaly on a multi-element mantle-normalized diagram (Fig. 10).

The reconstructed whole rocks show a wide range of Nb/La and Nb/Ta ratios, ranging from negative to strongly positive Nb and Ta anomalies (Fig. 10) (Rudnick et al., 2000). The jadeite-rich eclogites have high Sr/Nd (except KEC 81-7), whereas the jadeite-poor eclogites have approximately chondritic Sr/Nd ratios. Many eclogites have low abundances of Zr (and in some samples also low Hf) relative to Sm. This Zr depletion is not due to overlooked accessory phases such as zircon in the whole rock reconstruction because the measured whole rocks also show Zr depletions. All eclogites have low Th concentrations, low Th/U ratios, and relatively uniform Sr contents. The jadeite-rich eclogites have more heterogeneous trace element patterns than the jadeite-poor eclogites.

Ancient metasomatic enrichment, before the kimberlite-related alteration, is a mantle process that can significantly change the chemical composition of mantle-derived samples. Metasomatism by passing melts is expected to increase Mg# [molar Mg/(Mg + Fe)], Ba, Nb, Zr, and LREE contents of the original eclogite (Dawson, 1984; Harte, 1987; Zindler and Jagoutz, 1988; Ireland et al., 1994). Evidence of metasomatic enrichment of a LREE-depleted rock are sigmoidal and "double hump" cpx and/or whole rock REE patterns (Johnson et al., 1990; Ireland et al., 1994). Such REE patterns are predicted for early stages of metasomatism by melt percolation models (Navon and Stolper, 1987). The final results of porous flow are smooth, LREE-enriched patterns (Navon and Stolper, 1987; Takazawa et al., 1992). These re-enriched REE patterns cannot easily be distinguished from undepleted, enriched rocks once the re-enriched rock reaches trace element equilibrium at upper mantle conditions. The Koidu low MgO eclogites analyzed have smooth, LREE-depleted cpx and reconstructed whole rock REE patterns and are depleted to very depleted in other highly incompatible trace elements such Ba and Th. Furthermore, the Koidu eclogites have Mg# (45–71) that are significantly lower than the metasomatized eclogites of Ireland et al. (1994) (Mg# = 74) or primitive, peridotite-derived melts (Mg# 74–80). Thus, we conclude that garnet and cpx in the low MgO eclogites do not show evidence for equilibration or exchange with ancient metasomatic agents.

5. ORIGINS OF THE KOIDU LOW MGO ECLOGITES

The mafic compositions and lithospheric equilibration conditions of the Koidu low MgO eclogites could be the result of (1) mantle melting and crystallization of these magmas and their cumulates at high pressures ("mantle" hypothesis), (2) metamorphism and foundering of underplated basaltic magmas at the base of the continental crust, and (3) metamorphism ± partial melting of subducted oceanic crust. A number of observations lead us to favor the last hypothesis.

5.1. Primary Mantle Melts and Cumulates

In the "mantle" hypothesis, peridotite melting must have occurred at pressures exceeding 3 GPa, since pressure estimates of the low MgO eclogites cluster between 3.3 and 3.6 GPa (see above). However, the major element compositions of the Koidu low MgO eclogites differ significantly from primary, high-pressure mantle melts (Fig. 11). Mantle melting at high pres-

Table 7. Reconstructed whole rock compositions of the Koidu low MgO eclogites and the median low MgO eclogite.

	Median Low MgO eclogite	**KEC 80-A2** Low jadeite 0.68% rutile	**KEC 81-4** Low jadeite 0.62% rutile	**KEC 81-5** Low jadeite 0.66% rutile	**KEC 81-18** Low jadeite 0.65% rutile	**KEC 86-6** Low jadeite 0.6% rutile	**KEC 86-56** Low jadeite 0.7% rutile	**KEC 86-72B** Low jadeite 0.63% rutile
		c	wr	wr	wr	c	c	wr
Sc	42	48	40	40	47	48	57	45
Ti	4541	4541	4223	4293	4663	4028	6286	4526
V	297	352	n. d.	364	332	336	297	322
Cr	319	319	n. d.	715	326	305	339	320
Ni	125	179	n. d.	154	59	138	84	38
Sr	52	41	39	60	62	47	50	87
Y	17	17	18	20	17	14	20	15
Zr	21.7	9.8	19	14	24	24	27	27
Nb	0.75	12	0.09	0.16	0.64	0.20	0.87	27
La	0.55	0.26	1.1	0.69	0.61	0.14	0.35	0.86
Ce	2.1	1.3	3.3	2.0	2.5	1.1	1.7	3.5
Pr	0.43	0.36	n. d.	0.44	0.52	n. d.	n. d.	n. d.
Nd	3.1	2.8	4.0	3.1	3.4	2.8	2.8	3.9
Sm	1.6	1.5	1.7	1.6	1.7	1.4	1.7	1.7
Eu	0.59	0.57	0.59	0.64	0.64	0.50	0.72	0.64
Gd	2.4	2.2	2.4	2.6	2.4	2.0	3.0	2.4
Tb		0.41	n. d.	0.50	0.46	n. d.	n. d.	n. d.
Dy	3.2	2.9	3.4	3.8	3.2	2.4	3.8	2.7
Ho		0.60	0.77	0.81	0.69	n. d.	n. d.	n. d.
Er	2.1	1.8	2.3	2.5	2.1	1.6	2.4	1.6
Yb	1.9	1.7	2.2	2.2	1.9	1.5	2.2	1.6
Lu	0.30	0.27	0.38	0.32	0.30	0.22	0.33	0.23
Hf	0.94	0.54	0.88	0.72	1.00	1.11	0.94	1.1
Ta	0.036	0.26	0.003	0.015	0.028	0.026	0.060	0.26
Pb	0.15	n. d.	n. d.	n. d.	n. d.	0.06	0.06	0.14
Th	0.019	0.020	0.046	0.058	0.019	0.005	0.006	0.022
U	0.019	0.036	0.041	0.024	0.044	0.007	0.019	0.051

	K91-4 Low jadeite 1.07% rutile	**K91-22** Low jadeite 0.5% rutile	**KEC 81-3** High jadeite 0.42% rutile	**KEC 81-7** High jadeite 0.65% rutile	**KEC 81-8** High jadeite 0.82% rutile	**KEC 81-10A** High jadeite no rutile	**KEC 81-21** High jadeite no rutile	**K91-11** High jadeite 1.1% rutile
	c	c	wr	wr	wr	wr	wr	c
Sc	32	41	28	29	43	37	44	40
Ti	7266	3430	4608	5367	5367	2188	1928	7405
V	268	465	n. d.	239	399	226	263	269
Cr	396	249	n. d.	622	287	268	499	244
Ni	220	303	n. d.	79	125	75	197	103
Sr	45	50	68	45	70	31	61	52
Y	17	10	8.1	20	13	11	17	27
Zr	15.5	12.7	16	47	9.5	32.5	12.8	48.1
Nb	0.75	0.41	5.3	9.2	1.7	0.18	0.10	12
La	0.13	0.55	1.0	1.9	0.56	0.18	0.24	1.58
Ce	1.0	2.4	4.2	5.9	2.1	0.8	1.0	5.2
Pr	n. d.	n. d.	n. d.	0.95	0.42	0.17	n. d.	n. d.
Nd	3.2	3.4	4.2	5.4	2.6	1.3	1.1	5.0
Sm	2.3	1.2	1.5	2.1	1.1	0.8	0.6	2.4
Eu	0.92	0.44	0.58	0.81	0.41	0.39	0.31	0.87
Gd	3.5	1.6	1.9	3.1	1.4	1.5	1.5	3.8
Tb	n. d.	n. d.	n. d.	0.59	0.27	0.30	n. d.	n. d.
Dy	3.8	1.9	1.8	3.8	2.2	2.1	2.7	5.1
Ho	n. d.	n. d.	0.32	0.80	0.52	0.45	n. d.	n. d.
Er	2.0	1.2	0.88	2.3	1.7	1.3	2.2	3.4
Yb	1.9	1.1	0.75	2.1	1.8	1.4	2.3	3.3
Lu	0.27	0.17	0.11	0.32	0.28	0.22	0.36	0.47
Hf	0.67	0.94	0.68	1.6	0.50	1.11	0.47	1.58
Ta	0.092	0.013	0.066	0.27	0.013	0.023	0.007	0.090
Pb	0.11	0.17	n. d.	n. d.	n. d.	n. d.	0.12	0.65
Th	b. d.	0.038	0.037	0.013	0.025	0.004	0.006	0.047
U	0.007	0.016	0.055	0.061	0.080	0.007	0.001	0.037

(Continued)

Table 7. (Continued)

	K91-58 Low MgO 1.2% ilmenite	**KEC 86-KB-3** Kyanite-bearing 0.25% rutile	**KEC 86-GB-12** Graphite-bearing 1.2% rutile	**KEC 86-GB-70** Graphite-bearing 0.45% rutile
	c	c	c	c
Sc	38	19	46	35
Ti	5620	2212	8168	3987
V	424	142	286	175
Cr	112	228	263	643
Ni	66	144	58	136
Sr	54	26	75	78
Y	26	5.0	33	23
Zr	21.7	8.1	52	34
Nb	21	0.059	0.37	1.1
La	0.33	b. d.	0.50	1.2
Ce	1.3	0.10	2.1	2.7
Pr	n. d.	n. d.	n. d.	n. d.
Nd	2.2	0.87	3.5	2.5
Sm	1.6	0.56	2.3	1.1
Eu	0.71	0.31	0.89	0.47
Gd	2.9	0.79	4.6	2.0
Tb	n. d.	n. d.	n. d.	n. d.
Dy	5.0	1.0	5.8	3.6
Ho	n. d.	n. d.	n. d.	n. d.
Er	3.3	0.60	3.4	3.0
Yb	3.0	0.54	3.0	3.3
Lu	0.45	0.070	0.46	0.55
Hf	1.27	0.43	1.8	1.5
Ta	0.95	0.013	0.036	0.078
Pb	0.026	n. d.	0.22	0.40
Th	0.017	0.002	0.003	0.034
U	0.009	0.011	0.004	0.017

Concentrations are given in ppm (μg/g). Low jadeite = <30 mol.% jadeite in cpx. High jadeite = >30 mol.% jadeite in cpx. wr = modal amount of rutile calculated by mass balance using whole rock Ti contents. c = modal amount of rutile calculated assuming no Ti anomaly. See text for details. n. d. = not determined. b. d. = below detection limit. Mineral modes are published in Hills and Haggerty (1989) and Fung and Haggerty (1995). Reconstructed major element compositions are given in Fung and Haggerty or are calculated from the data in Fung and Haggerty.

sures generates picritic melts with higher MgO and lower Al_2O_3 and Na_2O contents than found in the Koidu low MgO eclogites. This is due to decreased stability of olivine and increased stability of garnet and jadeite with increasing pressure (Falloon and Green, 1988; Kinzler and Grove, 1992; Kushiro, 1996; Walter, 1998). The low Mg#s (45–71; only the diamond-bearing sample KEC 80-DB-3 (not analyzed here) has Mg# = 79) of the Koidu eclogites are considered primary, since both mantle metasomatism and partial melting will increase the Mg#. The protoliths of the low MgO eclogites were thus most likely evolved basaltic melts, because their Mg#s are generally too low to be primary mantle melts (Mg# 70–80). Similarly, their Ni contents are generally lower than observed in primary mantle melts (38–303 ppm vs. $\geq$ 320 ppm) (Frey et al., 1978). Note that MORBs (mid-ocean ridge basalts) and probably most Archean basalts are not simple low-pressure partial melts, but involve a component of higher pressure partial melting, and have evolved by significant olivine fractionation from more primitive liquids (e.g., Baker and Stolper, 1994). Cumulates from mantle melts will have even higher Mg#s and Ni contents than melts. For example, Taylor and Neal's (1989) Group A eclogites, which they interpreted as high pressure cumulates of a mantle melt along with trapped liquid, have Mg#s between 82 and 87, and Ni contents between 493 and 659 ppm.

The occurrence of kyanite and corundum in some low MgO eclogites also argues against an origin for the eclogites as crystallized primary melts or their cumulates (Jacob et al., 1998). During the early stages of melt formation and migration in the upper mantle, melts most likely migrate by porous flow and interact extensively with the wall rocks. That is, the melts are in equilibrium with peridotitic mantle. Kyanite-bearing eclogites, however, are not in equilibrium with peridotitic mantle at high pressures and would react with olivine to form aluminous pyroxene and garnet (Milholland and Presnall, 1998). Thus, if kyanite-bearing eclogites represent cumulates of fractionated high-pressure mantle melts, these melts must have been isolated from peridotite. If melts migrate in channels or fractures (conduits and dikes), it is possible that early cumulates precipitated on cool peridotite wallrocks serve to isolate magma from wallrocks, resulting in dikes that are mineralogically zoned (cf. pyroxenite dikes in ophiolites). In contrast to many pyroxenite xenolith suites (e.g., Irving, 1980; Wilshire et al., 1980), there is no evidence that the Koidu eclogites formed in this manner. Mineralogically zoned eclogites and composite xenoliths (eclogite cross-cutting peridotite) have not been found in the Koidu xenolith suite (Tompkins and Haggerty, 1984). On the other hand, kyanite is a common accessory phase in massif eclogites (apparent former ocean floor) in some Phanerozoic fold belts (e.g., Mottana et al., 1990). Moreover, the presence of positive Eu anomalies in kyanite-bearing eclogites presented in this study and in Taylor and Neal (1989),

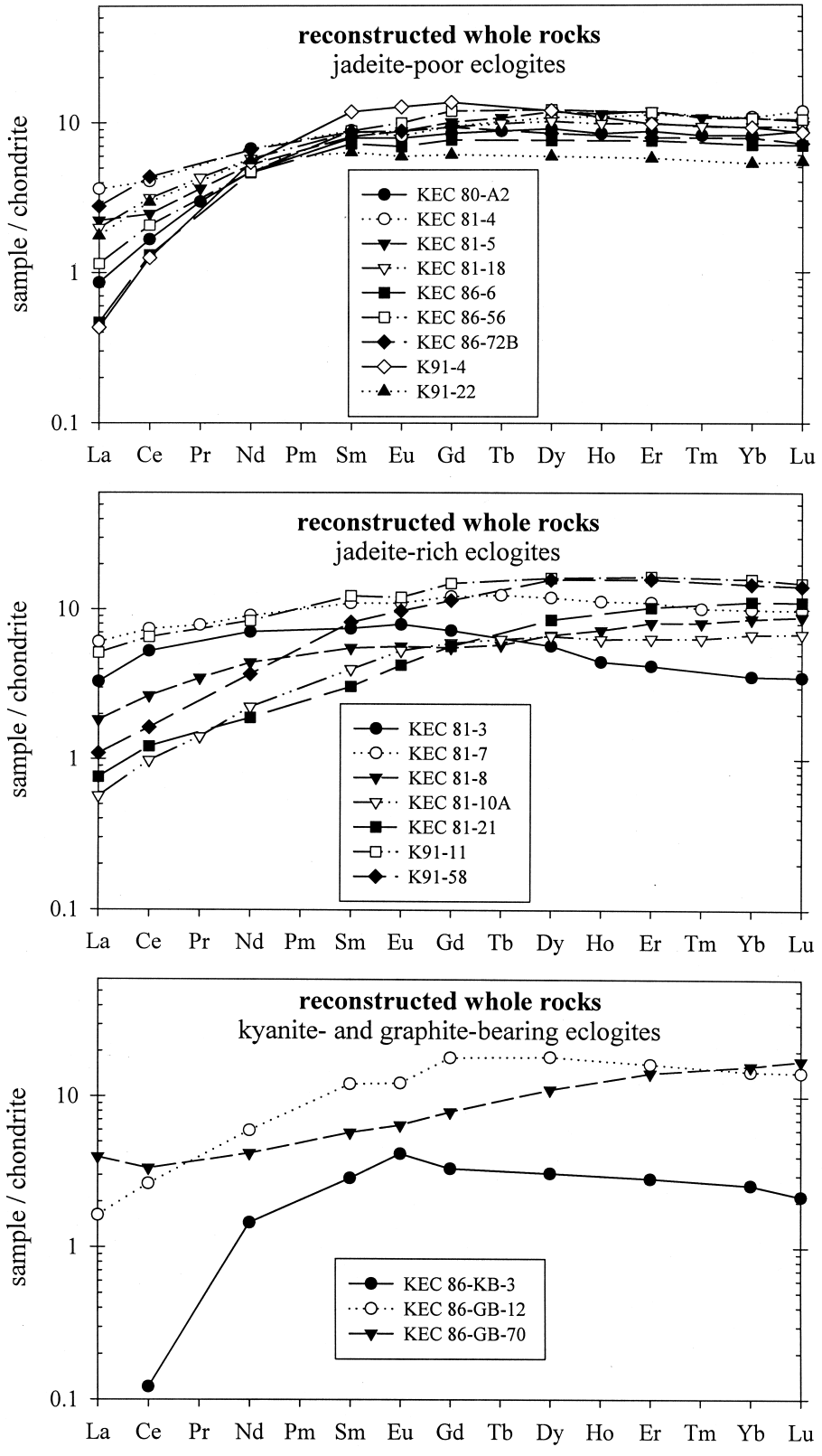

Fig. 9. Chondrite-normalized reconstructed whole rock REE data for Koidu low MgO eclogite xenoliths. Top: jadeite-poor eclogites (<30 mol.% jadeite in cpx). Middle: jadeite-rich eclogites (>30 mol.% jadeite in cpx). Bottom: kyanite- and graphite-bearing eclogites. Normalized as in Figure 2.

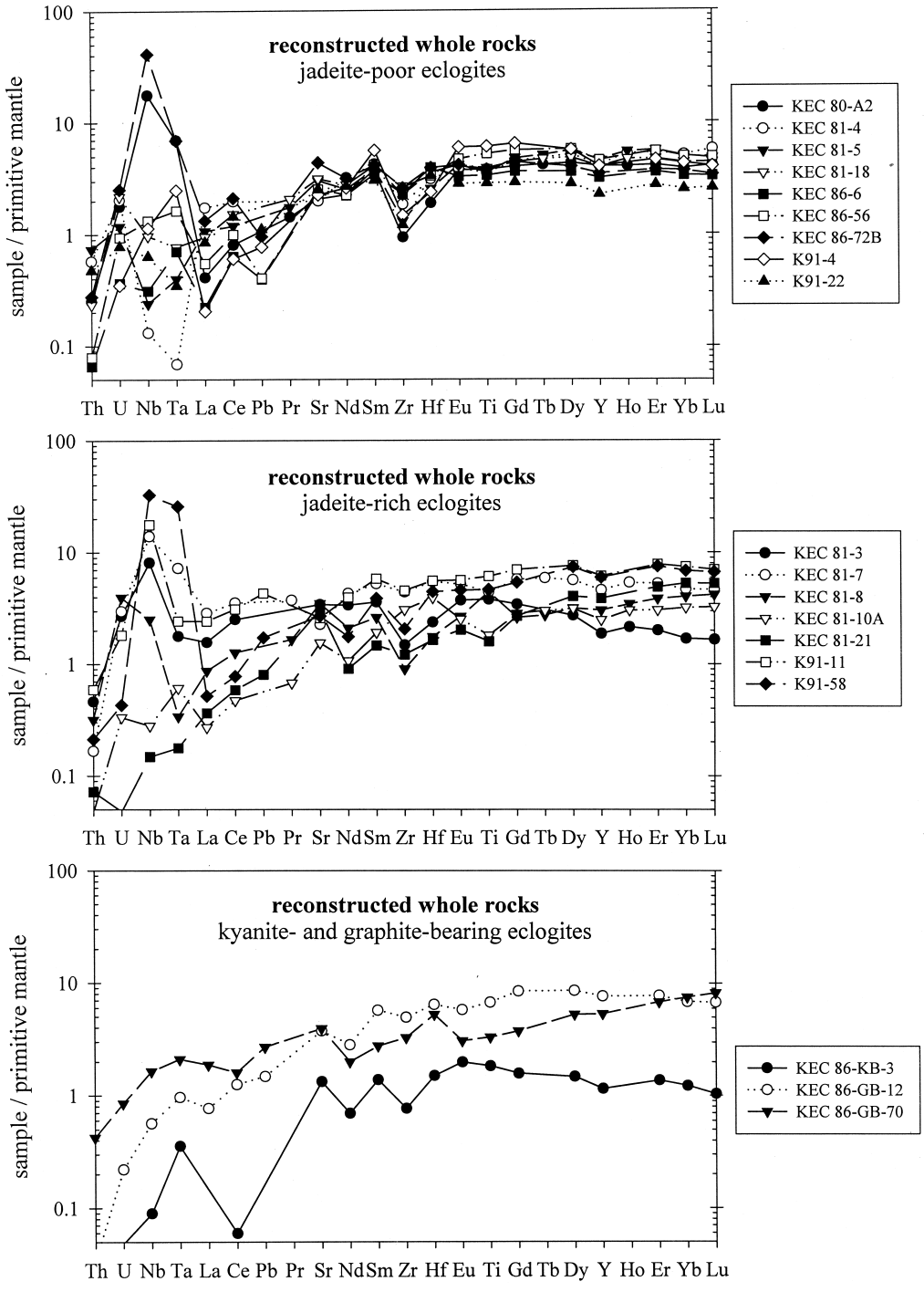

Fig. 10. Mantle-normalized reconstructed whole rock trace element diagrams for Koidu low MgO eclogite xenoliths. Top: jadeite-poor eclogites (<30 mol.% jadeite in cpx). Middle: jadeite-rich MgO eclogites (>30 mol.% jadeite in cpx). Bottom: kyanite- and graphite-bearing eclogites. Normalized as in Figure 3.

and negative Eu anomalies in graphite-bearing eclogites, point to accumulation and fractionation of plagioclase, respectively, and, therefore, to a shallow, crustal origin.

5.2. Underplated Basalts

Some eclogite xenoliths may represent basaltic magmas that underplated the lower continental crust and cooled into the eclogite facies at Moho depths (Pearson et al., 1991; El Fadili and Demaiffe, 1999). Although estimated equilibration pressures of the Koidu low MgO eclogites in excess of 2.8 GPa and the occurrence of diamond in some samples imply that these eclogites are derived from the lithospheric mantle (>100 km depth), it is conceivable that the eclogites represent former crustal material that has delaminated from the lower continental

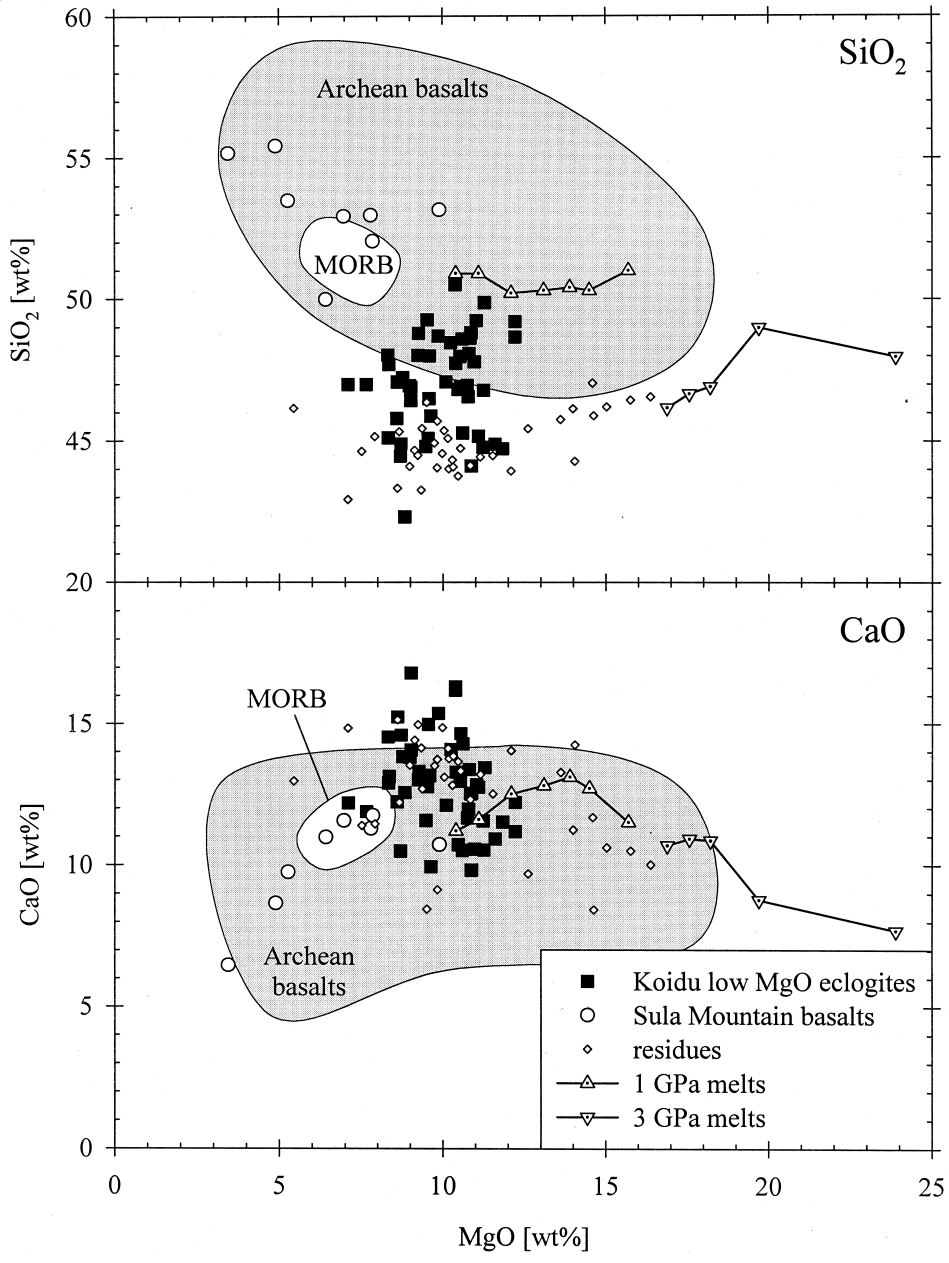

Fig. 11. Plots of SiO_2 and CaO vs. MgO whole rock content. Solid squares: reconstructed Koidu low MgO eclogites (Hills and Haggerty, 1989; Fung and Haggerty, 1995). Open circles: Sula Mountain greenstone belt basalts (Rollinson, 1997). Small diamonds: Residues from eclogite melting experiments (Carroll and Wyllie, 1990; Rapp and Watson, 1995; Sen and Dunn, 1994; Winther and Newton, 1991; Wolf and Wyllie, 1994), assuming equal proportions of residual garnet and cpx. Melts in equilibrium with eclogite have silicic to intermediate compositions (high Al_2O_3, trondhjemitic-tonalitic, granodioritic, quartz dioritic). Dotted triangles and reverse triangles: Experimental pyrolite melts at 1 and 3 GPa, respectively (Baker and Stolper, 1994; Walter, 1998). Gray field shows Archean basalts and komatiites compiled from the literature. White field depicts unaltered mid-ocean ridge basalt (MORB) from the RidgePet Database.

crust. A number of geochemical observations, however, are inconsistent with this interpretation. Neither crystal fractionation nor assimilation of continental crust is likely to account for the low $\delta^{18}O$ values observed in some of the low MgO eclogites. Contamination of basaltic magmas with continental crust increases $\delta^{18}O$ and could thus possibly explain eclogites with high $\delta^{18}O$, but these eclogites do not show any other indicators of crustal contamination such as negative Eu and Nb anomalies or high SiO_2 and incompatible trace element contents. We conclude that the Koidu eclogites are unlikely to represent foundered or delaminated lower continental crust.

5.3. Subducted Oceanic Crust

Stable isotopes (oxygen, carbon, and sulfur) are perhaps the most reliable tracers of rocks affected by low-temperature

processes that originated at near-surface conditions such as hydrothermal alteration. The large range of $\delta^{18}O$ values observed in many xenolithic eclogites can be explained by hydrothermal alteration of an oceanic crustal protolith (MacGregor and Manton, 1986; Neal et al., 1990; Jacob et al., 1994; Beard et al., 1996), similar to the $\delta^{18}O$ variations observed in ophiolite sequences (Gregory and Taylor, 1981; Muehlenbachs, 1986). The changing fractionation between seawater and basalt with increasing temperature (i.e., depth) causes heavy isotopic values ($\delta^{18}O > 5.5‰$) at low temperatures and shallow levels of the oceanic crust and light isotopic values ($\delta^{18}O < 5.5‰$) at greater depth where temperatures are higher. Recent studies have documented the preservation of these presubduction/collision oxygen isotope signatures of altered basalts and gabbros in massif eclogites and eclogite-facies rocks (e.g., Getty and Selverstone, 1994; Putlitz et al., 2000).

The Koidu low MgO eclogites have more variable oxygen isotopic compositions than mantle-derived peridotite xenoliths (Fig. 1). That is, $\delta^{18}O$ in garnet in the Koidu low MgO eclogites ranges from 4.68 to 6.78‰, averaging 5.48 ± 0.96‰ (2σ, $n = 31$), while garnet in peridotites derived from the lithospheric mantle averages 5.37 ± 0.36‰ ($n = 44$) (Mattey et al., 1994b). The variable $\delta^{18}O$ of the Koidu low MgO eclogites suggests a low-pressure protolith such as altered oceanic crust, although the absolute range in values is not as large as those observed in ophiolite sections.

Values of $\delta^{18}O$ of the low MgO eclogites do not correlate with major or trace elements, reflecting the heterogeneous nature of hydrothermal alteration and/or the protoliths of the eclogites. Garnets in the kyanite-bearing eclogites have low to normal $\delta^{18}O$ (4.73–5.35‰), suggestive of high-T alteration in the deeper, gabbroic parts of oceanic crust, which is consistent with their origin as plagioclase-rich cumulates. In addition, the correlation between jadeite content (hence bulk rock Na) and variability of highly incompatible trace elements suggests that the more jadeite-rich samples experienced more intensive hydrothermal alteration, although jadeite does not correlation with $\Delta^{18}O$ (Table 2).

The silica content of the low MgO eclogites is low compared with Archean basalts and present-day MORB (Fig. 11). The low silica content could be due to loss of a silicic melt (or fluid) during subduction, loss of SiO_2 during seafloor alteration, or a combination of these processes. Both low-T and high-T seafloor alteration result in stronger depletions of Ca than of SiO_2 in altered basalts (Ridley et al., 1994; Staudigel et al., 1996; Hart et al., 1999). The Koidu low MgO eclogites, however, do not show depletions in CaO relative to Archean basalts and present-day MORB (Fig. 11). We therefore favor partial melting and extraction of a silicic melt as an explanation for the low silica content of these eclogites. The similarity of the compositions of the Koidu eclogites and of residues derived from eclogite melting experiments (Winther and Newton, 1991; Sen and Dunn, 1994; Wolf and Wyllie, 1994; Rapp and Watson, 1995) and their distinct compositions when compared to Archean basalts and MORB (Fig. 11) supports this conclusion. Taken together, major element and oxygen isotope systematics suggest that the Koidu low MgO eclogites are derived from altered Archean oceanic crust that underwent an episode of partial melting or dehydration during subduction.

6. TRACE ELEMENT CHARACTERISTICS OF THE PROTOLITHS OF THE LOW MGO ECLOGITES

Elements that are not greatly affected by hydrothermal alteration and subduction zone metamorphism (conservative elements) can be utilized to determine the geochemical character of the protoliths of the eclogites. Elements commonly considered to be immobile during hydrothermal alteration, or at least only weakly mobile, include the trivalent HREEs, Y, TiO_2, and Al_2O_3, all of which have concentrations in hydrothermal fluids orders of magnitude lower than in oceanic crust (Ridley et al., 1994 and references therein). The HFSE are conserved during low-T alteration of the oceanic crust and change in abundance only by simple dilution/accumulation due to the mobility of other elements; Nb/Ta and Zr/Hf remain nearly constant (Staudigel et al., 1996). In contrast, the HFSE may dissolve under the low pH conditions of high-T hydrothermal solutions and may be enriched in altered samples where secondary (hydrothermal) rutile has precipitated (Ridley et al., 1994).

During shallow subduction, probably only H_2O, K, and Rb are significantly removed from the altered crust. Deeper subduction is likely to be more efficient in removing elements from the oceanic crust, but the relatively small amount of water available makes it difficult to change the composition of the downgoing slab significantly by this process (Staudigel et al., 1995 and references therein). Moreover, the HFSE and HREE will be largely retained by the residue if it contains rutile and garnet, respectively (Brenan et al., 1995; Stalder et al., 1998).

If the subducting oceanic crust is relatively warm, it may undergo partial melting. The most likely melting regions are associated with dehydration boundaries of the dominant hydrous phases in the subducted slab (Peacock, 1996). That is, dehydration melting is probably caused by amphibole breakdown and the formation of eclogite (Martin, 1986). During amphibole breakdown, Nb, Ta, and HREE are compatible in a rutile-bearing eclogitic residue, but Zr and Hf may be depleted (Rapp et al., 1999; Foley et al., 2000). Partial melting may change Nb/Ta, Zr/Hf, and Nb/La ratios but will not greatly affect the overall abundances of HREE. Partition coefficients for Nb and Ta between rutile-bearing eclogite and melt are close to unity (Rapp et al., 1999; Foley et al., 2000). Therefore, the Nb/Ta ratio may be fractionated if D_{Nb} and D_{Ta} are not equal, but the overall abundances of Nb and Ta in the residue will change only slightly. For example, 25% depletion of Ta is sufficient to change Nb/Ta from the chondritic value of 17.4 to the observed median value of the eclogites of 22.4 (see below).

Considering the above observations, the Nb, Ta, and HREE contents of the reconstructed rutile-bearing eclogites are likely to reflect the approximate content (probably within a factor of 2–3 for Nb and Ta) of these elements in the crustal precursor. If eclogites exhibit no Nb anomaly or have a positive anomaly, then the Nb concentration can be used to distinguish between incompatible element enriched and depleted precursor rocks. As few or no Archean magmas with positive Nb anomalies are known (Arndt et al., 1997), one can assume that trace elements with similar incompatibility (e.g., Th and La) had similar or higher normalized concentrations in the precursor.

To determine a representative trace element composition of the low MgO eclogites, we adopted the median value. This approach is justified because the low MgO eclogites represent

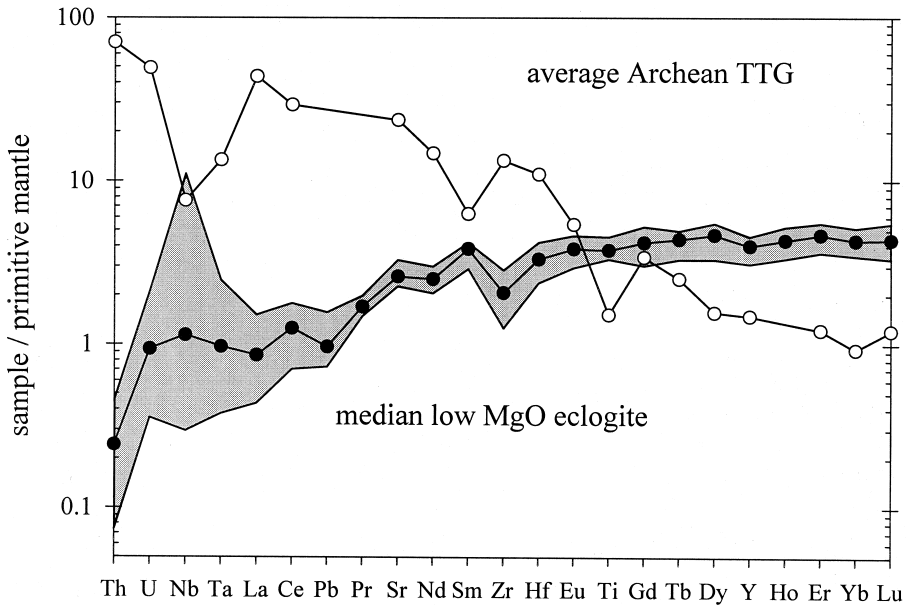

Fig. 12. Mantle-normalized trace element diagram for the median reconstructed whole rock low MgO eclogite (solid circles). Gray field shows the range of compositions between the first and third quartile. Open circles denote average Archean tonalite-trondhjemite-granodiorite suites (TTG) (Martin, 1994). Note the high Nb/La, Nb/Ta, and Sm/Zr ratios of the median eclogite and the complementary low Nb/La, Nb/Ta, and Sm/Zr ratios of the average Archean TTG. Normalized as in Figure 3.

a single population (cf. Fig. 1 in Rudnick et al., 2000). That is, the compatible trace elements (with respect to a rutile-bearing eclogite) such as the HREE show a normal distribution, while Nb, Ta, and incompatible trace elements (e.g., La) approximate a log-normal distribution. In both cases, the median coincides with the center of the distribution. The median of the reconstructed low MgO eclogites shows LREE depletion, a flat HREE pattern, high Sr/Nd, and a positive Nb anomaly (Table 7, Fig. 12). These features necessitate that the protoliths experienced an episode of partial melting or dehydration of rutile-bearing garnet amphibolite or eclogite during subduction. Based on major element chemistry, Rollinson (1997) proposed that the low MgO eclogites are residues left after 20% partial melting of a protolith similar to the Archean tholeiitic basalts from the Sula Mountains greenstone belt in Sierra Leone (Fig. 11). These late Archean basalts show REE patterns that are slightly LREE depleted to slightly LREE enriched (Rollinson, 1999). Partial melting or dehydration of the subducted basalt causes loss of LREE while a large portion of Nb and most of the HREE stay in the residue, due to the high partition coefficients of rutile and garnet, respectively (Fig. 13).

Conservative trace element compositions also suggest that the low MgO eclogites probably underwent an episode of partial melting rather than dehydration during subduction, as far as a distinction between both can be made (cf. Bureau and Keppler, 1999). The reconstructed eclogites have low Zr/Sm ratios and low Zr concentrations. During partial melting, $D_{Zr,Hf}^{rutile/melt}$ are one to two orders of magnitude lower than $D_{Nb,Ta}^{rutile/melt}$ (Rapp et al., 1999; Foley et al., 2000). In contrast, $D_{Zr,Hf}^{rutile/fluid}$ and $D_{Nb,Ta}^{rutile/fluid}$ are the same order of magnitude (Brenan et al., 1994; Stalder et al., 1998), suggesting that dehydration would not lead to Zr depletion. Another feature that suggests the eclogites are residues is the low concentration of Th (and to a lesser extent of U) observed in the median eclogite (Table 7). These elements are highly incompatible in clinopyroxene, garnet (Green, 1994 and references therein), and (presumably) rutile (except U^{6+}) during partial melting. In contrast, Th is considered to be immobile during dehydration of eclogite (Becker et al., 2000) and thus is not expected to be depleted by dehydration alone. Our median eclogite has an order of magnitude lower Th concentration than the model eclogite of Becker et al. (2000): 19 ppb vs. 168 ppb (cf. 187 ppb in MORB, Hofmann, 1988), which they interpret to represent dehydrated (subducted), altered MORB.

While the uncertainties of pressure and temperature of partial melting, melting reactions, and the exact composition of the protoliths preclude quantitative modeling, the following observations can be made from simple partial melting calculations (Fig. 13).

(1) The depleted trace element patterns of the Koidu eclogites can be reproduced by 15 to 40% batch melting (or lower degrees of continuous melting) of a basaltic protolith with a flat or slightly LREE-enriched trace element pattern. Such patterns are typical of greenstone belt basalts (e.g., Archean Sula Mountains basalts) (Rollinson, 1999) or oceanic plateau basalts. This degree of melting coincides with that required to form TTG as determined from eclogite melting experiments.

(2) The calculated residues have much lower Sr concentrations than the Koidu eclogites, suggesting that either residual plagioclase was present during partial melting (Martin, 1999) or that the precursor was enriched in Sr (perhaps due to alteration processes) compared to typical Archean tholeiitic basalts.

(3) Simple partial melting models fail to account for the

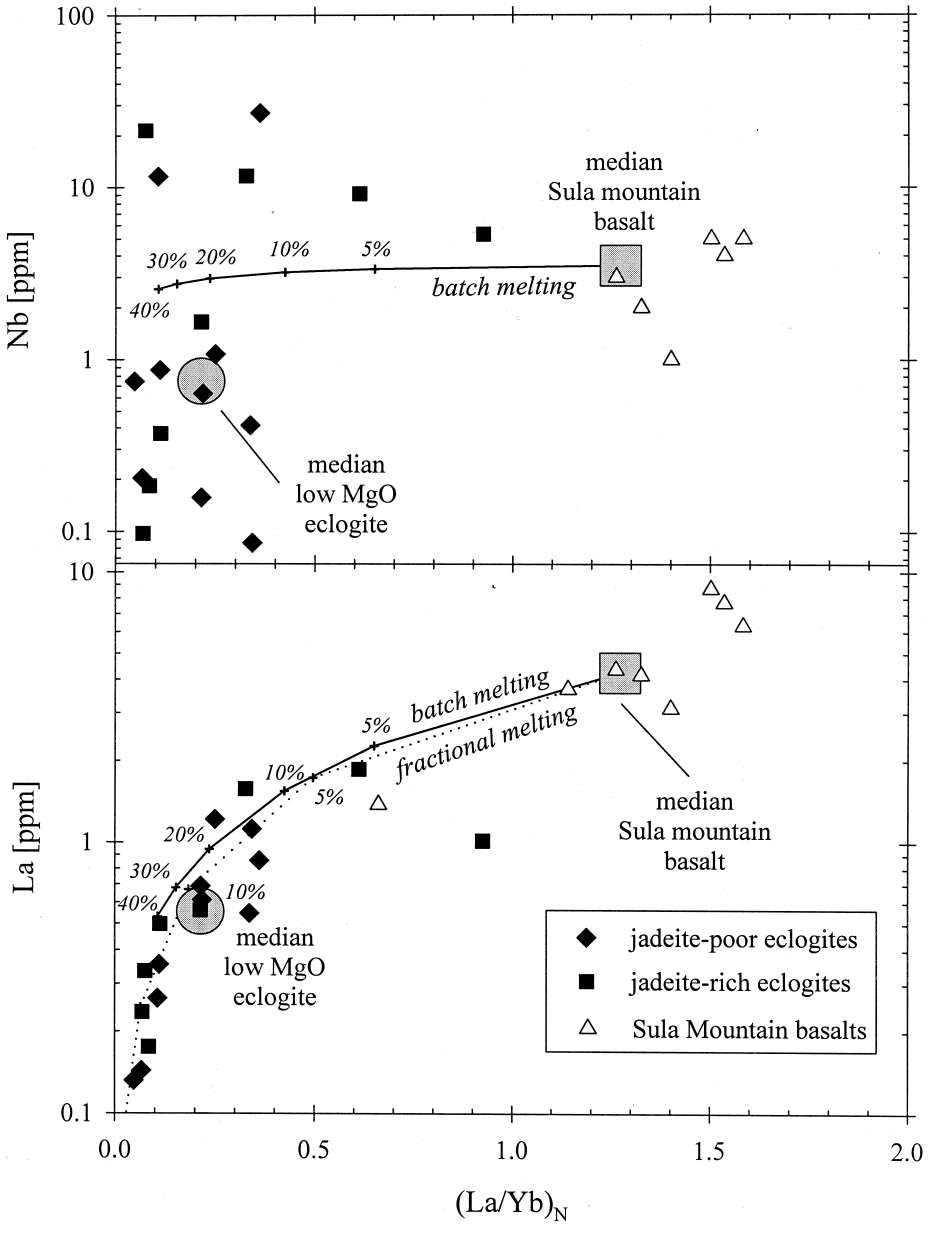

Fig. 13. Plot of the reconstructed whole rock Nb (top) and La (bottom) content vs. $(La/Yb)_N$ for the Koidu low MgO eclogites. Gray circles show the median low MgO eclogite composition (Table 7). Solid diamonds are jadeite-poor eclogites (<30 mol.% jadeite in cpx); solid squares are jadeite rich eclogites (>30 mol.% jadeite in cpx). Large gray squares depict the median composition of the Sula mountain greenstone belt basalts (Rollinson, 1997); open triangles depict individual basalt analyses. The lines illustrate possible partial melting trends where the eclogites get strongly depleted in La but only slightly depleted in Nb; the Nb and Yb contents remain approximately constant due to the high partition coefficients of rutile and garnet, respectively. Solid and dotted lines show batch and fractional melting, respectively. Numbers denote the degree of partial melting, assuming 0.5% rutile and a garnet/cpx ratio of 40:60 in the residue. Partition coefficients are taken from Barth et al. (1997), Foley et al. (2000), and Klein et al. (2000).

large range of Nb and Ta contents of the xenolith population (0.06–43 ppm Nb, 0.003–2.2 ppm Ta). Because Nb and Ta are slightly incompatible to slightly compatible in the bulk eclogite (depending on the modal amount of rutile and the partition coefficients appropriate for the pressure and temperature of partial melting), their concentrations in the residue remain comparatively constant during partial melting. Note that the Nb and Ta concentrations are not correlated with the calculated amount of rutile (see above), suggesting that the range of Nb concentrations cannot be caused by variable amounts of residual rutile alone. Thus, the wide range in concentrations may reflect basaltic protoliths with variable degrees of incompatible element enrichment. Alternatively, the variable Nb and Ta concentrations may be

caused by redistribution of HFSE during high-T seafloor alteration (Ridley et al., 1994), the dependence of D_{Nb} and D_{Ta} on melt composition, as observed in haplogranitic systems (Horng and Hess, 2000) or additional, yet unresolved, processes.

7. IMPLICATIONS FOR ARCHEAN CRUST GENERATION

The low MgO eclogites from Koidu, Sierra Leone, have variable oxygen isotopic compositions that exceed the mantle range and reconstructed trace element patterns that are depleted in Ba, Th, U, and light REE, but have a positive Nb anomaly. The Koidu low MgO eclogites may represent fragments of processed oceanic crust, which are residues from Archean continental crust formation. The subducted oceanic crust was partially melted to produce TTG suites, and thus created these residual eclogites, which were subsequently emplaced into the subjacent lithospheric environment.

The complementary silicic melt to the median low MgO eclogite is enriched in incompatible trace elements and has Nb and HREE depletions, as observed in TTG suites, which make up large portions of the crust in Archean cratons. TTGs also show high Zr/Sm and Th/U (Condie, 1993; Martin, 1994), complementary to the eclogites (Fig. 12). Therefore, the low MgO eclogites have the trace element characteristics expected for residues from TTG generation. This notion is supported by the restitic major element composition of these xenoliths (Fig. 11) (Rollinson, 1997). Thus, the Koidu low MgO eclogites may represent parts of the missing mafic reservoir needed to explain the silicic composition of the crust in Archean cratons. The volume of mafic residue produced during the production of TTGs exceeds by far the volume of mafic lower crust and eclogite in the lithospheric mantle currently present in Archean cratons (Ireland et al., 1994). During partial melting of subducted oceanic crust, portions of the residue (the oceanic crust of the slab) are likely to be transported deeper into the mantle, possibly all the way to the core-mantle boundary. The silicic melts rise (driven by the density contrast between melt and solids) and variably interact with the peridotitic mantle wedge on their way to the surface (Rudnick et al., 1994; Kelemen et al., 1998; Rapp et al., 1999), forming the Archean TTG suites (Martin, 1986). It is also likely that portions of the slab may be left behind in the lithosphere and later sampled by passing kimberlites (e.g., Valley et al., 1998).

Although the Koidu low MgO eclogites probably represent ancient altered oceanic crust that has been recycled in the mantle and partially melted at high pressures, this does not mean that the tectonic environment was exactly analogous to modern subduction zones, i.e., similar to slab melting and generation of adakites in the Aleutians, southern Andes, and Kamtchatka (Drummond et al., 1996; Kepezhinskas et al., 1997; Yogodzinski and Kelemen, 1998). An alternative scenario to slab melting is tectonic emplacement of oceanic crust in the lowermost continental crust and partial melting in the garnet stability field. Such overthickening of continental crust may be caused by terrain collision (e.g., de Wit, 1998) or could be associated with oceanic plateaux (Stein and Goldstein, 1996). Higher mantle temperatures in the Archean may have resulted in more buoyant slabs due to higher melt production at midocean ridges, thicker oceanic crust, and more depleted lithospheric mantle. If slabs were positively buoyant and difficult to subduct, a different tectonic style would have been necessary to remove heat from the Archean mantle (e.g., Davies, 1992). Rather than being subducted, oceanic crust might have accumulated over downwellings and, after cooling, "dripped" back into the mantle (Park, 1981; Campbell and Griffiths, 1992). Irrespective of the exact tectonic setting, the Koidu low MgO eclogites demonstrate recycling of oceanic crust and formation of Archean continental crust at convergent plate boundaries.

Acknowledgments—We thank Kate Tomford, April Larson, Bridget Sinnott, and Taylor Perron for help with sample preparation and mineral separation. Discussions with Debbie Hassler, Cin-Ty Lee, and Thomas Zack and reviews by Harry Becker and Dorrit Jacob helped to improve the manuscript. This study has been supported by NSF grants EAR 980467 to R.L.R.; EAR 9711008 to R.L.R. and W.F.M.; EAR 96-28260 and DOE 93ER14389 to J.W.V.; and EAR 98-05091 to S.E.H.

Associate editor: M. A. Menzies

REFERENCES

Arndt N. T., Albarède F., and Nisbet E. G. (1997) Mafic and ultramafic magmatism. In *Greenstone Belts* (ed. M. J. de Wit and L. D. Ashwal), pp. 233–254. Oxford University Press.

Baker M. B. and Stolper E. M. (1994) Determining the composition of high-pressure mantle melts using diamond aggregates. *Geochim. Cosmochim. Acta* **58,** 2811–2827.

Barth M. G., McDonough W. F., and Rudnick R. L. (2000) Tracking the budget of Nb and Ta in the continental crust. *Chem. Geol.* **165,** 197–213.

Barth M. G., Foley S. F., and Horn I. (1997) Experimental trace-element partitioning in tonalitic systems. *Seventh Ann. V.M. Goldschmidt Conference* **18**.

Barth M. G., Rudnick R. L., Carlson R. W., Horn I., and McDonough W. F. (1999) Geochronological Re-Os and U-Pb constraints on the eclogite-tonalite connection in the Archean Man Shield, West Africa. *EOS Trans. AGU* **80,** F1193.

Beard B. L., Fraracci K. N., Taylor L. A., Snyder G. A., Clayton R. A., Mayeda T. K., and Sobolev N. V. (1996) Petrography and geochemistry of eclogites from the Mir kimberlite, Yakutia, Russia. *Contrib. Mineral. Petrol.* **125,** 293–310.

Becker H., Jochum K. P., and Carlson R. W. (2000). Trace element fractionation during dehydration of eclogites from high-pressure terranes and the implications for element fluxes in subduction zones. *Chem. Geol.* **163,** 65–99.

Beckinsale R. D., Gale N. H., Pankhurst R. J., Macfarlane A., Crow M. J., Arthurs J. W., and Wilkinson A. F. (1980) Discordant Rb-Sr and Pb-Pb whole rock isochron ages for the Archaean basement of Sierra Leone. *Precambrian Res.* **13,** 63–76.

Blundy J. and Wood B. (1994) Prediction of crystal-melt partition coefficients from elastic moduli. *Nature* **372,** 452–454.

Boynton W. V. (1984) Cosmochemistry of the REE: Meteorite studies. In *REE geochemistry* (ed. P. Henderson). Elsevier.

Brenan J. M., Shaw H. F., Phinney D. L., and Ryerson F. J. (1994) Rutile-aqueous fluid partitioning of Nb, Ta, Hf, Zr, U and Th: Implications for high field strength element depletions in island-arc basalts. *Earth Planet. Sci. Lett.* **128,** 327–339.

Brenan J. M., Shaw H. F., Ryerson F. J., and Phinney D. L. (1995) Mineral-aqueous fluid partitioning of trace elements at 900°C and 2.0 Gpa: Constraints on the trace element chemistry of mantle and deep crustal fluids. *Geochim. Cosmochim. Acta* **59,** 3331–3350.

Bureau H. and Keppler H. (1999) Complete miscibility between silicate melts and hydrous fluids in the upper mantle: Experimental evidence and geochemical implications. *Earth Planet. Sci. Lett.* **165,** 187–196.

Campbell I. H. and Griffiths R. W. (1992) The changing nature of mantle hotspots through time: Implications for the chemical evolution of the mantle. *J. Geol.* **92,** 497–523.

Caporuscio F. A. and Smyth J. R. (1990) Trace element crystal chemistry of mantle eclogites. *Contrib. Mineral. Petrol.* **105,** 550–561.

Carroll M. R. and Wyllie P. J. (1990) The system tonalite-H_2O at 15 kbar and the genesis of calc-alkaline magmas. *Am. Mineral.* **75,** 345–357.

Clayton R. N., Goldsmith J. R., Karel K., Mayeda T. K., and Newton R. C. (1975) Limits on the effect of pressure on isotopic fractionation. *Geochim. Cosmochim. Acta* **39,** 1197–1201.

Condie K. C. (1993) Chemical composition and evolution of the upper continental crust: Contrasting results from surface samples and shales. *Chem. Geol.* **104,** 1–37.

Coplen T. B. (1996) New guidelines for reporting stable hydrogen, carbon, and oxygen isotope-ratio data. *Geochim. Cosmochim. Acta* **60,** 3359–3360.

Davies G. F. (1992) On the emergence of plate tectonics. *Geology* **20,** 936–966.

Dawson J. B. (1984) Contrasting types of upper-mantle metasomatism. In *Kimberlites II: The mantle and crust-mantle relationships* (ed. J. Kornprobst), pp. 289–294. Elsevier.

de Wit M. J. (1998) On Archean granites, greenstones, cratons and tectonics: Does the evidence demand a verdict? *Precambrian Res.* **91,** 181–226.

Deines P. and Haggerty S. E. (2000). Small-scale oxygen isotope variations and petrochemistry of ultradeep (> 300 km) and transition zone xenoliths. *Geochim. Cosmochim. Acta* **64,** 117–131.

Drummond M. S., Defant M. J., and Kepezhinskas P. K. (1996) Petrogenesis of slab-derived trondhjemite-tonalite-dacite/adakite magmas. *Trans. Royal Soc. Edinburgh, Earth Sci.* **87,** 205–215.

Eggins S. M., Woodhead J. D., Kinsley L. P. J., Mortimer G. E., Sylvester P., McCulloch M. T., Hergt J. M., and Handler M. R. (1997) A simple method for the precise determination of >40 trace elements in geological samples by ICPMS using enriched isotope internal standardisation. *Chem. Geol.* **134,** 311–326.

El Fadili S. and Demaiffe D. (1999) Petrology of eclogite and granulite nodules from the Mbuji Mayi kimberlites (Kasai, Congo): Significance of kyanite-omphacite intergrowths. In *Proceedings of the 7th International Kimberlite Conference*, Vol. 1 (ed. J. J. Gurney, J. L. Gurney, M. D. Pascoe, and S. H. Richardson), pp. 205–213. Red Roof Design cc.

Ellis D. J. and Green D. H. (1979) An experimental study of the effect of Ca upon garnet-clinopyroxene Fe-Mg exchange equilibria. *Contrib. Mineral. Petrol.* **71,** 13–22.

Falloon T. J. and Green D. H. (1988) Anhydrous partial melting of peridotite from 8 to 35 kbar and the petrogenesis of MORB. *J. Petrol.* 379–414.

Foley S. F., Barth M. G., and Jenner G. A. (2000) Rutile/melt partition coefficients for trace elements and an assessment of the influence of rutile on the trace element characteristics of subduction zone magmas. *Geochim. Cosmochim. Acta* **64,** 933–938.

Frey F. A., Green D. H., and Roy S. D. (1978) Integrated models of basalt petrogenesis: A study of quartz tholeiites to olivine melilitites from southeastern Australia utilizing geochemical and experimental petrological data. *J. Petrol.* **19,** 463–513.

Fung A. T. and Haggerty S. E. (1995) Petrography and mineral compositions of eclogites from the Koidu Kimberlite Complex, Sierra Leone. *J. Geophys. Res.* **100,** 20,451–20,473.

Getty S. R. and Selverstone J. (1994) Stable isotopic and trace element evidence for restricted fluid migration in 2 GPa eclogites. *J. metamorphic Geol.* **12,** 747–760.

Green T. H. (1994) Experimental studies of trace-element partitioning applicable to igneous petrogenesis-Sedona 16 years later. *Chem. Geol.* **117,** 1–36.

Gregory R. T. and Taylor H. P. (1981) An oxygen isotope profile in a section of Cretaceous oceanic crust, Samail ophiolite, Oman: Evidence for $\delta^{18}O$ buffering of the oceans by deep (>5 km) seawater-hydrothermal circulation at mid-ocean ridges. *J. Geophys. Res.* **86,** 2737–2755.

Haggerty S. E. (1983) The mineral chemistry of new titanates from the Jagersfontein kimberlite, South Africa: Implications for metasomatism in the upper mantle. *Geochim. Cosmochim. Acta* **47,** 1833–1854.

Hart S. R., Blusztajn J., Dick H. J. B., Meyer P. S., and Muehlenbachs K. (1999) The fingerprint of seawater circulation in a 500-meter section of ocean crust gabbros. *Geochim. Cosmochim. Acta* **63,** 4059–4080.

Harte B. (1987) Metasomatic events recorded in mantle xenoliths: An overview. In *Mantle Xenoliths* (ed. P. H. Nixon), pp. 625–640. John Wiley & Sons.

Harte B. and Kirkley M. B. (1997) Partitioning of trace elements between clinopyroxene and garnet: Data from mantle eclogites. *Chem. Geol.* **136,** 1–24.

Helmstaedt H. and Doig R. (1975) Eclogite nodules from kimberlite pipes of the Colorado Plateau-Samples of subducted Franciscan-type oceanic lithosphere. *Phys. Chem. Earth* **9,** 95–111.

Hills D. V. and Haggerty S. E. (1989) Petrochemistry of eclogites from the Koidu Kimberlite Complex, Sierra Leone. *Contrib. Mineral. Petrol.* **103,** 397–422.

Hofmann A. W. (1988) Chemical differentiation of the Earth: The relationship between mantle, continental crust, and oceanic crust. *Earth Planet. Sci. Lett.* **90,** 297–314.

Horn I., Rudnick R. L., and McDonough W. F. (2000) Precise elemental and isotopic ratio determination by combined solution nebulization and laser ablation ICP-MS: Application to U/Pb geochronology. *Chem. Geol.* **164,** 281–301.

Horng W. S. and Hess P. C. (2000). Partition coefficients of Nb and Ta between rutile and anhydrous haplogranite melts. *Contrib. Mineral. Petrol.* **138,** 176–185.

Ireland T. R., Rudnick R. L., and Spetsius Z. (1994) Trace elements in diamond inclusions from eclogites reveal link to Archean granites. *Earth Planet. Sci. Lett.* **128,** 199–213.

Irving A. J. (1980) Petrology and geochemistry of composite ultramafic xenoliths in alkalic basalts and implications for magmatic processes within the mantle. *Am. J. Sci.* **280A,** 389–426.

Jacob D., Jagoutz E., Lowry D., Mattey D., and Kudrjavtseva G. (1994) Diamondiferous eclogites from Siberia: Remnants of archean oceanic crust. *Geochim. Cosmochim. Acta* **58,** 5195–5207.

Jacob D., Jagoutz E., Lowry D., and Zinngrebe E. (1998) Comment on 'The origins of Yakutian eclogite xenoliths' by G. A. Snyder, L. A. Taylor, G. Crozaz, A. N. Halliday, B. L. Beard, V. N. Sobolev, and N. V. Sobolev. *J. Petrol.* **39,** 1527–1533.

Jacob D. E. and Foley S. F. (1999) Evidence for Archean ocean crust with low high field strength element signature from diamondiferous eclogite xenoliths. *Lithos* **48,** 317–336.

Jerde E. A., Taylor L. A., Crozaz G., Sobolev N. V., and Sobolev V. N. (1993) Diamondiferous eclogites from Yakutia, Siberia: Evidence for a diversity of protoliths. *Contrib. Mineral. Petrol.* **114,** 189–202.

Johnson K. T., Dick H. J. B., and Shimizu N. (1990) Melting in the oceanic upper mantle: An ion microprobe study of diopsides in abyssal peridotites. *J. Geophys. Res.* **95,** 2661–2678.

Kellemann P. B., Hart S. R., and Bernstein S. (1998) Silica enrichment in the continental upper mantle via melt/rock reaction. *Earth Planet. Sci. Lett.* **164,** 387–406.

Kepezhinskas P., McDermott F., Defant M. J., Hochstaedter A., Drummond M. S., Hawkesworth C. J., Koloskov A., Maury R. C., and Bellon H. (1997) Trace element and Sr-Nd-Pb isotopic constraints on a three-component model of Kamchatka Arc petrogenesis. *Geochim. Cosmochim. Acta* **61,** 577–600.

Kinzler R. J. and Grove T. L. (1992) Primary magmas of mid-ocean ridge basalts 1. Experiments and methods. *J. Geophys. Res.* **97,** 6885–6906.

Klein M., Stosch H. G., Seck H. A., and Shimizu N. (2000). Experimental partitioning of high field strength and rare earth elements between clinopyroxene and garnet in andesitic to tonalitic systems. *Geochim. Cosmochim. Acta* **64,** 99–115.

Kohn M. J. and Valley J. W. (1998) Effects of cation substitutions in garnet and pyroxene on equilibrium oxygen isotope fractionations. *J. metamorphic Geol.* **16,** 625–639.

Kushiro I. (1996) Partial melting of a fertile mantle peridotite at high pressures: An experimental study using aggregates of diamond. In *Earth processes: Reading the isotopic code*, Vol. 95 (ed. A. Basu and S. Hart), pp. 109–122. American Geophysical Union.

Longerich H. P., Jackson S. E., and Günther D. (1996) Laser ablation inductively coupled plasma mass spectrometric transient signal data acquisition and analyte concentration calculation. *J. Anal. At. Spectrom.* **11,** 899–904.

Macfarlane A., Crow M. J., Arthurs J. W., Wilkinson A. F., and Aucott

J. W. (1981) The geology and mineral resources of northern Sierra Leone. *Overseas Mem. Inst. Geol. Sci.* **7,** 103. p.
MacGregor I. D. and Manton W. I. (1986) Roberts Victor eclogites: Ancient oceanic crust. *J. Geophys. Res.* **91,** 14,063–14,079.
Martin H. (1986) Effect of steeper Archean geothermal gradient on geochemistry of subduction-zone magmas. *Geology* **14,** 753–756.
Martin H. (1994) The Archean grey gneisses and the genesis of continental crust. In *Archean Crustal Evolution* (ed. K. C. Condie), pp. 205–259. Elsevier.
Martin H. (1999) Adakitic magmas: Modern analogues of Archaean granitoids. *Lithos* **46,** 411–429.
Mattey D., Lowry D., and Macpherson C. (1994a) Oxygen isotope composition of mantle peridotite. *Earth Planet. Sci. Lett.* **128,** 231–241.
Mattey D. P., Lowry D., Macpherson C. G., and Chazot G. (1994b) Oxygen isotope composition of mantle minerals by laser fluorination analysis: Homogeneity in peridotites, heterogeneity in eclogites. *Mineral. Mag.* **58A,** 573–574.
McCandless T. E. and Gurney J. J. (1989) Sodium in garnet and potassium in clinopyroxene: Criteria for classifying mantle eclogites. In *Kimberlites and related rocks*, Vol. 2 (ed. J. Ross), pp. 827–832. Blackwell Scientific.
McCormick T. C., Smyth J. R., and Caporuscio F. A. (1994) Chemical systematics of secondary phases in mantle eclogites. In *Kimberlites, related rocks and mantle xenoliths*, Vol. 1 (ed. H. O. A. Meyer and O. H. Leonardos), pp. 405–419. CPRM.
McDonough W. F. and Sun S. S. (1995) Composition of the Earth. *Chem. Geol.* **120,** 223–253.
Milholland C. S. and Presnall D. C. (1998) Liquidus phase relations in the CaO-MgO-Al_2O_3-SiO_2 system at 3.0 GPa: The aluminous pyroxene thermal divide and high-pressure fractionation of picritic and komatiitic magmas. *J. Petrol.* **39,** 3–27.
Mottana A., Carswell D. A., Chopin C., and Oberhänsli R. (1990) Eclogite facies mineral parageneses. In *Eclogite Facies Rocks* (ed. D. A. Carswell), pp. 16–52. Blackie.
Muehlenbachs K. (1986) Alteration of the oceanic crust and the ^{18}O history of seawater. In *Stable isotopes in high temperature geological processes* (ed. J. W. Valley, H. P. J. Taylor, and J. R. O'Neil), pp. 425–444. Mineralogical Society of America.
Navon O. and Stolper E. (1987) Geochemical consequences of melt percolation: The upper mantle as a chromatographic column. *J. Geol.* **95,** 285–308.
Neal C. R., Taylor L. A., Davidson J. P., Holden P., Halliday A. N., Nixon P. H., Paces J. B., Clayton R. N., and Mayeda T. K. (1990) Eclogites with oceanic crustal and mantle signatures from the Bellsbank kimberlite, South Africa, part 2: Sr, Nd, and O isotope geochemistry. *Earth Planet. Sci. Lett.* **99,** 362–379.
Park R. G. (1981) Origin of horizontal structure in high-grade Archaean terrains. In *Archean geology*, Vol. 7 (ed. J. E. Glover and D. I. Groves), pp. 481–490.
Peacock S. M. (1996) Thermal and petrologic structure of subduction zones. In *Subduction top to bottom* (ed. G. E. Bebout, D. W. Scholl, S. H. Kirby, and J. P. Platt), pp. 119–133. AGU.
Pearce N. J. G., Perkins W. T., Westgate J. A., Gorton M. P., Jackson S. E., Neal C. R., and Chenery S. P. (1997) A compilation of new and published major and trace element data for NIST SRM 610 and NIST SRM 612 glass reference materials. *Geostand. Newslett.* **21,** 115–144.
Pearson N. J., O'Reilly S. Y., and Griffin W. L. (1991) The granulite to eclogite transition beneath the eastern margin of the Australian craton. *Eur. J. Mineral.* **3,** 293–322.
Putlitz B., Matthews A., and Valley J. W. (2000). Oxygen and hydrogen isotope study of high-pressure metagabbros and metabasalts (Cyclades, Greece): Implications for the subduction of oceanic crust. *Contrib. Mineral. Petrol.* **138,** 114–126.
Rapp R. P., Shimizu N., Norman M. D., and Applegate G. S. (1999) Reaction between slab-derived melts and peridotite in the mantle wedge: Experimental constraints at 3.8 GPa. *Chem. Geol.* **160,** 335–356.
Rapp R. P. and Watson E. B. (1995) Dehydration melting of metabasalts at 8–32 kbar: Implications for continental growth and crust-mantle recycling. *J. Petrol.* **36,** 891–931.
Reid J. E., Horn I., Longerich H. P., Forsythe L., and Jenner G. A. (1999) Determination of Zr and Hf in a flux-free fusion of whole rock samples using laser ablation inductively coupled plasma-mass spectrometry (LA-ICP-MS) with isotope dilution calibration. *Geostand. Newslett.* **23,** 149–155.
Ridley W. I., Perfit M. R., Jonasson I. R., and Smith M. F. (1994) Hydrothermal alteration in oceanic ridge volcanics: A detailed study at the Galapagos fossil hydrothermal field. *Geochim. Cosmochim. Acta* **58,** 2477–2494.
Rollinson H. R. (1978) Zonation of supracrustal relics in the Archaean of Sierra Leone, Liberia, Guinea and Ivory Coast. *Nature* **272,** 440–442.
Rollinson H. (1997) Eclogite xenoliths in west African kimberlites as residues from Archaean granitoid crust formation. *Nature* **389,** 173–176.
Rollinson H. (1999) Petrology and geochemistry of metamorphosed komatiites and basalts from the Sula Mountains greenstone belt, Sierra Leone. *Contrib. Mineral. Petrol.* **134,** 86–101.
Rosenbaum J. M. and Mattey D. (1995) Equilibrium garnet-calcite oxygen isotope fractionation. *Geochim. Cosmochim. Acta* **59,** 2839–2842.
Rudnick R. L., Barth M., Horn I., and McDonough W. F. (2000). Rutile-bearing refractory eclogites: The missing link between continents and depleted mantle. *Science* **287,** 278–281.
Rudnick R. L., McDonough W. F., and Orpin A. (1994) Northern Tanzanian peridotite xenoliths: A comparison with Kaapvaal peridotites and inferences on metasomatic interactions. In *Kimberlites, related rocks and mantle xenoliths* (ed. H. O. A. Meyer and O. H. Leonardos), pp. 336–353. CPRM.
Rudnick R. L. and Nyblade A. A. (1999) The thickness and heat production of Archean lithosphere: Constraints from xenolith thermobarometry and surface heat flow. In *Mantle petrology: Field observations and high pressure experimentation: A tribute to Francis R. (Joe) Boyd* (ed. Y. Fei, C. M. Bertka, and B. O. Mysen), pp. 3–12. The Geochemical Society.
Schulze D. J., Valley J. W., Viljoen K. S., Stiefenhofer J., and Spicuzza M. (1997) Carbon isotope composition of graphite in mantle eclogites. *J. Geol.* **105,** 379–386.
Sen C. and Dunn T. (1994) Dehydration melting of a basaltic composition amphibolite at 1.5 and 2.0 GPa: Implications for the origin of adakites. *Contrib. Mineral. Petrol.* **117,** 394–409.
Smyth J. R., Caporuscio F. A., and McCormick T. C. (1989) Mantle eclogites: Evidence of igneous fractionation in the mantle. *Earth Planet. Sci. Lett.* **93,** 133–141.
Snyder G. A., Taylor L. A., Beard B. L., Crozaz G., Halliday A. N., Sobolev V. N., and Sobolev N. V. (1998) Reply to a comment by D. Jacob et al. on 'The origins of Yakutian eclogite xenoliths.' *J. Petrol.* **39,** 1535–1543.
Snyder G. A., Taylor L. A., Crozaz G., Halliday A. N., Beard B. L., Sobolev V. N., and Sobolev N. V. (1997) The origins of Yakutian eclogite xenoliths. *J. Petrol.* **38,** 85–113.
Stalder R., Foley S. F., Brey G. P., and Horn I. (1998) Mineral-aqueous fluid partitioning of trace elements at 900–1200°C and 3.0–5.7 GPa: New experimental data for garnet, clinopyroxene, and rutile, and implications for mantle metasomatism. *Geochim. Cosmochim. Acta* **62,** 1781–1801.
Staudigel H., Davies G. R., Hart S. R., Marchant K. M., and Smith B. M. (1995) Large scale isotopic Sr, Nd and O isotopic anatomy of altered oceanic crust: DSDP/ODP sites 417/418. *Earth Planet. Sci. Lett.* **130,** 169–185.
Staudigel H., Plank T., White B., and Schmincke H. U. (1996) Geochemical fluxes during seafloor alteration of the basaltic upper oceanic crust: DSDP Sites 417 and 418. In *Subduction top to bottom* (ed. G. E. Bebout, D. W. Scholl, S. H. Kirby, and J. P. Platt), pp. 19–38. AGU.
Stein M. and Goldstein S. L. (1996) From plume head to continental lithosphere in the Arabian-Nubian shield. *Nature* **382,** 773–778.
Takazawa E., Frey F. A., Shimizu N., Obata M., and Bodinier J. L. (1992) Geochemical evidence for melt migration and reaction in the upper mantle. *Nature* **359,** 55–58.
Taylor L. A. and Neal C. R. (1989) Eclogites with oceanic crustal and mantle signatures from the Bellsbank kimberlite, South Africa, Part I: Mineralogy, petrography, and whole rock chemistry. *J. Geol.* **97,** 551–567.
Taylor W. R., Tompkins L. A., and Haggerty S. E. (1994) Comparative

geochemistry of West African kimberlites: Evidence for a micaceous kimberlite endmember of sublithospheric origin. *Geochim. Cosmochim. Acta* **58,** 4017–4037.

Tompkins L. A. and Haggerty S. E. (1984) The Koidu Kimberlite Complex, Sierra Leone: Geological setting, petrology and mineral chemistry. In *Kimberlites; I, Kimberlites and related rocks*, Vol. 11A (ed. J. Kornprobst), pp. 83–105. Elsevier.

Valley J. W., Kinny P. D., Schulze D. J., and Spicuzza M. J. (1998) Zircon megacrysts from kimberlite; oxygen isotope variability among mantle melts. *Contrib. Mineral. Petrol.* **133,** 1–11.

Valley J. W., Kitchen N., Kohn M. J., Niendorf C. R., and Spicuzza M. J. (1995) UWG-2, a garnet standard for oxygen isotope ratios: Strategies for high precision and accuracy with laser heating. *Geochim. Cosmochim. Acta* **59,** 5223–5231.

Walter M. J. (1998) Melting of garnet peridotite and the origin of komatiite and depleted lithosphere. *J. Petrol.* **39,** 29–60.

Williams H. R. (1978) The Archaean geology of Sierra Leone. *Precambrian Res.* **6,** 251–268.

Wilshire H. G., Pike J. E. N., Meyer C. E., and Schwarzman E. C. (1980) Amphibole-rich veins in lherzolite xenoliths, Dish Hill and Deadman Lake, California. *Am. J. Sci.* **280A,** 576–593.

Winther K. T. and Newton R. C. (1991) Experimental melting of hydrous low-K tholeiite: evidence on the origin of Archean cratons. *Bull. Geol. Soc. Denmark* **39,** 213–228.

Wolf M. B. and Wyllie P. J. (1994) Dehydration-melting of amphibolite at 10 kbar: The effects of temperature and time. *Contrib. Mineral. Petrol.* **115,** 369–383.

Wood B. J. and Blundy J. D. (1997) A predictive model for rare earth element partitioning between clinopyroxene and anhydrous silicate melt. *Contrib. Mineral. Petrol.* **129,** 166–181.

Yogodzinski G. M. and Kelemen P. B. (1998) Slab melting in the Aleutians: Implications of an ion probe study of clinopyroxene in primitive adakite and basalt. *Earth Planet. Sci. Lett.* **158,** 53–65.

Zindler A. and Jagoutz E. (1988) Mantle cryptology. *Geochim. Cosmochim. Acta* **52,** 319–333.